Title:

Cellular mechanisms underlying beneficial versus detrimental effects of bacterial antitumor immunotherapy

Authors:

Jesse Garcia Castillo[1,3], Sebastian Fernandez[2,3], Timothy Campbell[1,3], Diego Gonzalez-Ventura[1], Jacob Williams[1], Julia Ybarra[1], Nicole Flores Hernandez[1], Elina Wells[1], Daniel A. Portnoy[1,2], and Michel DuPage[1]

Affiliations:

[1] Division of Immunology and Molecular Medicine, Department of Molecular and Cell Biology, University of California, Berkeley, Berkeley, CA 94720, USA

[2] Department of Plant and Microbiology, University of California, Berkeley, Berkeley, CA 94720, USA

[3] These authors contributed equally

Contact info: dupage@berkeley.edu

Summary:

Bacteria engineered to express tumor antigens as a cancer vaccine have yielded mixed results. Here, we utilized an attenuated strain of *Listeria monocytogenes* (*ΔactA, Lm*) that does not express tumor antigen to explore the immunological response to *Listeria* itself in the context of intravenous (IV), intratumoral (IT), or a combination of IV+IT administration into tumor-bearing mice. Unexpectedly, we found that *Lm* persisted in tumors of immune competent mice, regardless of the administration route. While IT *Lm* alone led to the recruitment of immunosuppressive immune cells that promoted tumor growth, IV *Lm* followed by IT *Lm* controlled tumor growth. IV *Lm* vaccination generated a pool of anti-*Lm* cytotoxic CD8 T cells that killed *Lm*-infected non-tumor cells to control tumor growth both indirectly, by limiting cancer cell proliferation, and directly, by enhancing tumor-specific T cell responses. Our findings reveal a differential impact of IT *Lm* administration on tumor progression that depends on the presence of anti-*Lm* CD8 T cells, which alone are sufficient to promote therapeutic efficacy.

Introduction:

At the turn of the 20th century, William Coley was the first to demonstrate the efficacy and application of bacterial cancer immunotherapies through combinations of intratumoral and systemic injections of cultured bacteria (gram-positive *Streptococci* and gram-negative *Serratia*) into patients with bone and soft-tissue sarcomas[1–3]. Today,

local tumoral administration of Bacillus Calmette-Guerin (BCG), a live attenuated strain of the gram-positive intracellular pathogen *Mycobacterium bovis*, by intravesical injection is a standard of care for non-muscle-invasive bladder cancer and the only FDA approved remnant of bacterial cancer therapy[4]. Recently, the discovery that bacteria naturally colonize many solid tumors has uncovered the potential of bacteria to serve as a drug delivery system or even as a cancer detection probe[5–16]. Improved methods to genetically manipulate bacterial genomes has also made it feasible to engineer bacteria that express tumor antigens, cytokines or cytotoxic proteins to control cancer[17–21]. Hence, multiple breakthroughs in manipulating bacteria and their activity in the tumor microenvironment has reignited interest in the potential for effective bacterial-based cancer immunotherapies.

Listeria monocytogenes engineered to express tumor-associated antigens and injected intravenously has effectively controlled multiple cancer models in mice[22–26]. To date, *Listeria* engineered to express tumor antigens and injected intravenously is the most tested bacterial-based immunotherapy in clinical trials for cancer[27]. Despite strong evidence of the vaccine's capacity to safely generate tumor antigen-specific CD8 T cells, the anti-cancer efficacy in patients has been mixed[28–33]. While several trials have shown improved outcomes in patients with otherwise untreatable cancers, such as malignant pleural mesothelioma or cervical cancer[28,30], many *Listeria*-based vaccine trials have not shown significant improvement in tumor control compared to standards of care. Therefore, it is critically important to discern why these vaccines fail despite generating antitumor CD8 T cells. In contrast to other bacterial cancer therapies, whether *Listeria* directly colonizes tumors has not been adequately investigated, likely because colonization was never a goal for its use against cancer in patients. A better understanding of the dynamics of *Listeria* interaction with host immune cells, its migration, and its persistence in tissues may reveal vulnerabilities of the current *Listeria*-based strategies as well as lead to improved uses of *Listeria* as an immune adjuvant directly within tumors.

Effective antitumor immunity requires a robust pool of antitumor immune cells and a permissive tumor microenvironment (TME) that allows for antitumor immune cells to function[17,34–36]. However, the TME is often highly immunosuppressive, allowing cancer cells to evade the immune system despite the presence of tumor-specific cytotoxic CD8 T cells[37–40]. Suppressive immune cell populations such as regulatory T cells (Tregs) or myeloid derived suppressor cells (MDSCs) have been investigated as major obstacles that give rise to the immunosuppressive TME and counteract antitumor mechanisms by immunotherapies[4142]. Thus, the failure of *Listeria* vaccines might be due to *Listeria's* singular use as a vaccine to generate antitumor CD8 T cells, without harnessing its capacity to stimulate the innate arm of the immune system and reverse immunosuppression directly within tumors. *Listeria* is rich in mechanisms to stimulate innate immunity directly in tumors[43]. Direct intratumoral injection of bacteria or bacterial

78 products may have underlied the success of William Coley's early therapies[44]. Recent
79 preclinical studies as well as clinical trials have demonstrated the feasibility and efficacy
80 of direct intratumoral injection of immune adjuvants naturally generated by *Listeria* and
81 other bacterial species that can activate host cell pattern recognition receptors (PRRs)
82 and stimulate the innate immune response against tumors[19,45–47]. However, there is a
83 lack of understanding as to how these adjuvants or bacteria in the TME directly impact
84 the tumor microenvironment by impacting different populations of immune cells.
85 Here, we show that either intratumoral (IT) or intravenous (IV) injection of *ΔactA*-
86 attenuated *Listeria* (*Lm*) that is not engineered to express tumor antigens did not control
87 tumor growth. Instead, IT *Lm* promoted tumor progression and *Lm* persisted
88 predominantly in polymorphonuclear cells (PMNs) within the TME. *Lm* persistence in
89 tumors was the result of IT *Lm* recruiting PMNs into the TME where they were polarized
90 into a myeloid-derived suppressor cell phenotype (PMN-MDSC) that could suppress
91 antitumor CD8 T cells[48,49]. In contrast, prior vaccination of mice against *Lm* by IV
92 injection, either early in tumor development or prior to tumor initiation, led to strong
93 tumor control upon IT *Lm* administration, even against highly aggressive sarcomas from
94 genetically engineered mice. Tumor control required IFNγ and TNFα production as well
95 as perforin-mediated killing by CD8 T cells specific to *Lm* antigen, which eliminated
96 PMN-MDSCs harboring *Lm* within the TME. Killing of *Lm*-infected host cells mediated
97 significant tumor control by reducing tumor cell proliferation and enhancing infiltration of
98 antitumor CD8 T cells. In addition, the IV+IT dosing regimen increased the infiltration
99 and reduced exhaustion phenotypes in tumor-specific CD8 T cells that further
100 contributed to tumor control, especially at later time points after the IV+IT *Lm* regimen.
101 Altogether, these results show that generating a localized anti-bacterial CD8 T cell
102 response in tumors is sufficient to overcome the suppressive TME and inhibit tumor
103 growth. Importantly, this work redefines the goals for effective anti-cancer bacterial
104 therapies by revealing a critical role for direct T cell targeting of conserved bacterial
105 antigens, which is more broadly applicable and rapidly translatable compared to
106 engineering bacteria to express patient-tailored, tumor-specific neoantigens. These
107 findings are fundamental to developing new and improved bacterial-based cancer
108 therapies.
109
110 **Results**
111
112 **Intratumoral injection of attenuated *Listeria* increases tumor growth.**
113 Immune adjuvants (i.e. PRR agonists) alone can be effective against cancers
114 when delivered directly into tumors without the addition of engineered tumor
115 antigens[45,50] . To test whether antitumor responses could be generated by direct
116 intratumoral (IT) injection of an attenuated strain of *L. monocytogenes*, which is not

117 engineered to express tumor-specific antigens, we used an *ΔactA* mutant, denoted *Lm*,
118 which contains the primary attenuating mutation used in many *Listeria* vaccine trials in
119 patients[51]. *ΔactA Listeria* lack the ActA virulence factor, making the bacteria unable to
120 polymerize host actin and spread from cell to cell, but importantly, *Lm* can still escape
121 from phagosomes and grow in the host cell cytosol, making it a potent inducer of MHC-
122 I-restricted CD8 T cell responses[52]. The *ΔactA* mutation renders *Lm* 1,000-10,000-fold
123 less virulent than WT *L. monocytogenes* without decreasing its capacity to induce CD8
124 T cells. This feature has led to its use in many *Listeria*-based clinical trials due to its
125 increased safety in patients[28,29,31,32]. However, the direct injection of *Listeria* into tumors
126 of cancer patients has never been tested. We performed dose-escalating experiments
127 with IT *Lm*, from $5x10^5$-$5x10^7$ CFUs, into tumors 11 days post tumor inoculation, when
128 tumors just became palpable (50-100mm^3), and found no lethality at a dose of $5x10^7$
129 *Lm*. Therefore, we used $5x10^7$ CFUs for IT *Lm* injections in all experiments. IT injection
130 of *Lm* did not result in tumor control in either MC38 or B16F10 tumor models but instead
131 led to a significant increase in tumor growth **(Figures 1A-1C, Figures S1A-1B).** This
132 result was unexpected, as *Lm* has been widely tested in experimental mouse models
133 and was not observed to cause increased tumor growth. However, IT injection of *Lm*
134 was never tested, so we hypothesized that this route of administration might be
135 responsible for increased tumor growth. Therefore, we tested the impact of *Lm*
136 administration on tumor growth after intravenous (IV) delivery, the most common
137 method of administration, of $1x10^6$ *Lm* (a lower dose was required to prevent lethality by
138 an IV route)[22]. In this scenario, we found no increase in tumor growth of B16F10 or
139 MC38 tumors, nor did we observe tumor growth control using the *Lm* strain **(Figures
140 S1C-1E)**. This finding is significant, as the route of *Lm* inoculation, IT versus IV, appears
141 to convert *Lm* from either being detrimental or potentially therapeutic for the control of
142 cancer.
143
144 ***Lm* colonizes tumors and persists in immunocompetent mice.**
145 We hypothesized that the varying impacts on tumor growth after IT compared to
146 IV *Lm* routes of administration could be due to varying *Lm* colonization in lymphoid
147 organs or the tumor itself. To examine the localization of *Lm* in tumor-bearing mice after
148 IV or IT *Lm* administration, we measured colony forming units (CFUs) for living bacteria
149 from various tissues harvested from tumor-bearing mice at several time points after *Lm*
150 administration. We found that *Lm* was cleared from spleens, lymph nodes, and liver by
151 5-10 days post injection in tumor-bearing mice, regardless of the route of delivery

152 **(Figures 1D-E)**. However, *Lm* colonized subcutaneous MC38 and B16F10 tumors for
153 up to 15 days, when experiments must end due to uncontrolled tumor growth (**Figures**
154 **1D-E**). *Lm* also colonized orthotopic pancreatic ductal adenocarcinomas (PDAC) after
155 IV injection (**Figure 1F**)[53]. While other bacterial species have been shown to persist in
156 tumors of mice, the persistence of live *Lm* within tumors of immunocompetent mice
157 long-term (more than 3-5 days) has not been documented. The colonization and
158 persistence of *Lm* in multiple tumor types after IV administration also revealed that
159 systemically delivered *Lm* can seed, grow, and colonize tumors long-term, even if
160 tumors are not easily accessible for direct IT injection.
161
162 ***Lm* infects PMN-MDSCs in tumors.**
163 We hypothesized that the distribution of *Lm* in specific cells of the tumor
164 microenvironment after IT administration shaped the immune response to promote
165 tumor growth. Because *Lm* is a facultative intracellular pathogen which primarily resides
166 in host cells after infection, we sought to identify which cells harbor bacteria in the
167 tumors of *Lm*-treated mice. To monitor intracellular infection of host cells by *Lm*, we
168 used a fluorescent-protein based system wherein a Tag-RFP reporter was expressed
169 under the control of the *actA* promoter in *ΔactA Listeria*, denoted *Lm-RFP* (**Figure**
170 **2A**)[54]. Since the *actA* promoter is induced more than 100-fold when *Lm* enters the host
171 cell cytosol, expression of Tag-RFP indicates that the bacteria have entered the cytosol
172 of a cell[55]. We observed co-localization of the RFP signal exclusively in $CD45^+$ immune
173 cells from single cell suspensions of MC38 or B16F10 tumors infected with *Lm-RFP*.
174 Notably, we did not observe RFP fluorescence in $CD45^-$ cells, which includes tumor
175 cells (**Figure 2B**).
176 Next, we tracked which types of $CD45^+$ immune cells harbored *Lm* in their
177 cytosol. At 4-and 24-hours post-infection, we observed an enrichment of RFP-
178 expressing bacteria in phagocytic immune cells, especially $Ly6G^+$ polymorphonuclear
179 (PMN) cells in both MC38 and B16F10 tumors models (**Figures 2C and S2A-D**)**.** To a
180 lesser extent, *Lm-RFP* was detected in $F4/80^+$ macrophages, $Ly6C^+$ monocytes, and
181 $CD11c^+$MHC-II^+ dendritic cells (**Figures 2C and S2B**). This distribution of *Lm* in
182 phagocytic immune cells, primarily PMNs and macrophages, was maintained after the
183 initial infection for up to five days (**Figure 2D**). However, in comparison to tumors at
184 steady state, IT *Lm* only induced a significant influx of PMNs into tumors, whereas other
185 phagocytic cell frequencies were unchanged (**Figures 2E and S2C-E)**. The RFP^+ PMNs
186 also increased between 4 and 24 hours after IT delivery (**Figure 2F and S2F**).
187 To rule out that *Lm* was phagocytosed during the single cell preparation for flow
188 cytometry analysis, we performed several experiments. First, we used confocal
189 microscopy of frozen tumor sections and also observed cytosolic RFP+ *Lm* within
190 Ly6G+ PMNs that aggregated in clusters within tumors (**Figure 2G and Figure S2G**).
191 Second, we prepared single cells from tumors in the presence of the antibiotic

192 gentamicin - to kill extracellular *Lm*, FACS purified Ly6G$^+$ PMNs, and performed
193 microscopic analysis of cytospun cells **(Figure 2H)**. We observed cytosolic RFP+ *Lm* in
194 Ly6G$^+$ PMNs by fluorescence microscopy with anti-Ly6G and by separate Gram
195 staining **(Figure 2I)**. Altogether, these results demonstrate that PMNs serve as a
196 reservoir for *Lm* in tumors after IT injection. These results were unanticipated, as we
197 expected PMNs would rapidly kill phagocytosed *Lm*, preventing their escape into the
198 cytosol and the expression of RFP[56–58].
199
200 **IT *Lm* recruits PMNs that differentiate into pro-tumorigenic PMN-MDSCs within**
201 **the tumor microenvironment.**
202 We hypothesized that the colonization and persistence of *Lm* in the cytosol of
203 PMNs was the result of PMN differentiation into myeloid derived suppressor cells
204 (MDSCs) within tumors, which could also promote tumor progression by inhibiting T cell
205 responses[32,59–61]. Phenotyping of PMNs at 4 and 24 hours after IT *Lm* revealed a
206 dynamic increase in the frequency of PMNs expressing the prototypical PMN-MDSC
207 marker CD14, and CD14 positivity was enriched in RFP$^+$ cells (**Figures 3A-B and S3A-**
208 **B**)[62]. To further confirm differentiation of PMNs into MDSCs within tumors, we sorted
209 Ly6G$^+$ PMNs from MC38 tumors and analyzed the expression of additional genes
210 known to be upregulated in MDSCs by qPCR. We observed that Ly6G$^+$ cells sorted
211 from tumors had higher expression of *Cd274*, *Cd14*, and *Vegfa* transcripts in
212 comparison to their counterparts sorted from the spleen or bone marrow (**Figure 3C).**
213 These results suggest that *Lm* infection within tumors recruits PMNs that then
214 differentiate into an MDSC phenotype in tumors, which may make them a permissive
215 reservoir for *Lm* colonization.
216 To test whether PMN-MDSCs become permissive to *Lm* growth in their cytosol
217 compared to PMNs, we used conditionally immortalized neutrophils (CINs) or primary
218 bone marrow progenitors differentiated into PMNs *in vitro* (**Figures 3D and S3C**)[61,63].
219 First, CIN-derived PMNs treated with conditioned supernatants from MC38 or B16F10
220 tumor cells increased expression of CD14 and PD-L1 relative to noncancerous,
221 immortalized NIH 3T3 cells, indicative of a PMN-MDSC phenotype (**Figures 3D-E**). As
222 a positive control, PMNs were differentiated into PMN-MDSCs by adding IL-6 and GM-
223 CSF, which led to a similar induction of CD14 and PD-L1 in CINs and bone marrow
224 derived PMNs (**Figures 3D** and **S3C**)[63]. To test whether the adoption of this MDSC
225 phenotype increased susceptibility to *Lm* infection, we infected heterogeneous PMN
226 cultures *in vitro* with *Lm-RFP* and monitored infection by flow cytometry. The CD14$^+$
227 PMNs were almost exclusively associated with *Lm* cytosolic infection as determined by
228 RFP expression (**Figures 3F and S3D**). These results strongly suggest that IT *Lm*
229 recruits PMNs to tumors where they become converted into PMN-MDSCs that allow for
230 *Lm* to infect and persist intracellularly in PMN-MDSCs.

231 PMN-MDSCs are widely associated with decreased antitumor immunity and
232 increased tumor progression. MDSCs have been shown to promote tumor growth by
233 inhibiting antitumor CD8 T cell responses[35,64]. To test whether PMN-MDSCs inhibited
234 CD8 T cells to promote cancer progression, we co-cultured tumor-specific $CD8^+$ T cells
235 (*in vitro* activated OT-I T cells) with OVA-expressing MC38 tumor cells in the presence
236 of PMNs sorted from spleens or MC38 tumors. The addition of $Ly6G^+$ PMNs from
237 tumors (PMN-MDSCs), but not spleens, led to a significant reduction in IFNγ cytokine
238 production from OT-I T cells in response to direct recognition of OVA-expressing MC38
239 tumors (**Figure 3G-H).** Next, we tested whether the depletion of all PMNs prior to IT Lm
240 infection could reverse enhanced tumor progression (**Figure 3I**). Indeed, depletion of
241 $Ly6G^+$ cells prevented increased tumor growth with IT *Lm* **(Figures 3J** and **Figure**
242 **S3E-F).** Notably, anti-Ly6G had no effect on tumor growth if mice were not administered
243 IT *Lm*. Interestingly, PMN depletion did not reduce bacterial colonization of tumors as
244 measured by CFU analysis (**Figure S3G**), although, using *Lm-RFP*, we found *Lm* was
245 now present primarily in macrophages (**Figure S3H**). These results support that IT *Lm*
246 recruits PMNs to tumors where they are converted to a MDSC phenotype that promotes
247 increased tumor growth. Therefore, *Lm* injection into tumors can promote tumor growth,
248 warranting caution when using bacterial cancer therapies.
249
250 **A combination of IV+IT *Lm* leads to tumor control across multiple cancer models.**
251 As neither IV nor IT administration of *Lm* alone provided strong tumor control, we
252 considered that both routes of infection together might generate therapeutic efficacy.
253 We reasoned that IV injection of *Lm* would effectively generate adaptive T cell
254 responses against *Lm*[65], and that subsequent IT *Lm* injection would then recruit anti-*Lm*
255 T cells into tumors to augment the antitumor immune response. To test this hypothesis,
256 we inoculated mice with MC38 or B16F10 tumors and administered *Lm* IV four days
257 later. At 11 days after tumor inoculation, when tumors were palpable, we injected *Lm* IT
258 into tumors as done previously with IT *Lm* alone **(Figure 4A)**. This combination of IV *Lm*
259 followed by IT *Lm* administration now significantly controlled both MC38 and B16F10
260 tumors **(Figures 4B-C and Figure S4A-B)**. Tumor control was evident by 9 days after
261 IT *Lm* injection, and tumors remained controlled throughout the experiment. Overall, of
262 the experiments performed, only IV+IT *Lm* administration led to tumor rejection (20% of
263 mice, 8 out of 40) and tumor rejection was never observed with IV or IT *Lm* alone.
264 Because IV administration of *Lm* also led to colonization of tumors (**Figure 1E)**, we
265 tested whether a second IV administration of *Lm* could also control tumors without
266 requiring direct IT *Lm* injection. We found that IV+IV also controlled tumors at two
267 different doses of IV *Lm* (**Figure S4C).** These results indicate that a second dose of *Lm*
268 IT or IV can control tumors after colonizing tumors without requiring the *Lm* strain to
269 express tumor antigens. In addition, we found that while $Ly6G^+$ PMNs were recruited
270 equally to tumors one day after IT *Lm* administration in both the IV+IT and IT-only *Lm*

271 dosing regimens, the frequency of Ly6G$^+$ cells was significantly reduced by 5 days after
272 IT *Lm* administration in the IV+IT setting **(Figure 4D)**. Furthermore, the fraction of
273 CD14$^+$ PMNs was almost completely abolished 5 days after IT *Lm* administration in the
274 IV+IT *Lm* dosing regimen, a reduction even below their frequency in PBS-treated control
275 tumors despite their robust increase 24 hours after IT *Lm* **(Figure 4E)**. Finally, when we
276 depleted PMNs prior to IT *Lm* administration in the IV+IT *Lm* regimen, we did not
277 observe any enhancement in tumor control, suggesting that the PMN reductions with
278 IV+IT *Lm* are sufficient to prevent PMN-MDSC promotion of tumor growth after the IT
279 *Lm* dose in the IV+IT therapeutic regimen **(Figure S4D)**.
280 Next, we wanted to establish whether *Lm* persisted in tumors in the setting of
281 IV+IT *Lm* administration. While *Lm* persisted in approximately 80% of IV+IT *Lm*-treated
282 tumors for up to 10 days after IT *Lm* administration, *Lm* was ultimately cleared from
283 tumors, with CFUs dropping to below the level of detection between days 15-20 after IT
284 *Lm* (day 21-30 of tumor growth) **(Figure 4F)**. We hypothesized that the clearance of *Lm*
285 from tumors was the result of *Lm*-specific T cells that were generated by IV *Lm* and then
286 recruited to tumors when *Lm* was injected IT. Therefore, tumor control with the IV+IT *Lm*
287 dosing could be the result of the recruitment of *Lm*-specific T cells to tumors.
288 Alternatively, because *Lm* colonized and persisted within the TME after IV
289 administration at day 4 (**Figure S1F**), the early seeding of tumors might contribute to
290 tumor control by changing the TME to augment the second IT injection of *Lm* in the
291 IV+IT regimen. To address this possibility, we performed experiments in which IV *Lm*
292 was administered prophylactically, 20 days prior to tumor inoculation (**Figure 4G**). In
293 this setting, *Lm* was completely cleared from mice prior to tumor inoculation and
294 therefore absent from tumors when IT *Lm* was administered. Now we could test whether
295 recalled *Lm*-specific adaptive immune cells, rather than changes in the distribution or
296 amount of *Lm* in tumors, was responsible for the antitumor efficacy of the IV+IT
297 regimen. This experiment showed clearly that mice injected with *Lm* prophylactically
298 (memory IV+IT) controlled tumors equivalently to the standard IV+IT regimen **(Figures**
299 **4H** and **S4E)**. However, prophylactic IV *Lm* injection alone, or IV *Lm* followed by a
300 subcutaneous injection of *Lm* on the contralateral flank of mice (memory IV+SQ), did
301 not control tumors **(Figure 4H)**. These results suggested that IT administration of *Lm*
302 mediated antitumor immunity by recalling an adaptive immune response against *Lm*
303 locally within the tumor.
304 Finally, we tested the IV+IT *Lm* dosing regimen in a clinically relevant mouse
305 sarcoma model - the tumor type most often treated by Coley, and a clinically relevant
306 model amenable to direct IT injections[1,23,66]. Using an aggressive *Kras*$^{G12D/+}$*;p53*$^{fl/fl}$-
307 generated orthotopic sarcoma model[67], we found that memory IV+IT *Lm* led to
308 significant sarcoma control from *Lm*-treated sarcomas compared to tumors treated with
309 PBS that had received IV *Lm* prophylactically **(Figures 4I and S4F)**. Together, these

310 results showed that IV+IT *Lm* can clear *Lm* from tumors and control tumor growth in a
311 manner that is not recapitulated with IV or IT *Lm* administrations alone.
312
313 **CD8 T cells are required for tumor control and *Lm* clearance with the IV+IT *Lm***
314 **dosing regimen.**
315 The reduction of tumor growth that occurred during the IV+IT *Lm* treatment
316 regimen compared to single-dose IV or IT *Lm* administrations suggested that an
317 adaptive immune response mediated tumor control. We hypothesized that T cells were
318 the critical adaptive immune cells important for tumor control in the IV+IT dosing
319 regimen due to their established role in both anti-*Lm* and antitumor immunity[65,68,69].
320 Indeed, flow cytometric analysis of tumors 5-8 days after IT *Lm* injection (early) revealed
321 an increase in the frequencies of both intratumoral CD8 and CD4 T cells in mice
322 receiving IV+IT *Lm* compared to IV-only or IT-only *Lm* injections or PBS control
323 injections (**Figures 5A-C, S5A-B**). Examination of tumors at the endpoint of tumor
324 growth (15-20 days after IT *Lm* injection, late) also revealed a significant increase in the
325 infiltration of CD8 T cells, but not a significant increase in CD4 T cells, in tumors of mice
326 treated with IV+IT *Lm* compared to other groups (**Figures 5A-C, S5A-B**). Intratumoral
327 regulatory T cells (Tregs) that are known to be immunosuppressive in the TME, were
328 not significantly reduced with the IV+IT regimen compared to IV or IT alone, although
329 they were reduced compared to the PBS treated mice (**Figures S5C-D**)[17,34–36,70–72].
330 Next, we assessed the functionality of the CD8 T cells by IFNγ and TNFα production 8
331 days after IT *Lm* or PBS injection. Here, the IV+IT *Lm* dosing regimen significantly
332 increased CD8 T cells production of IFNγ, but especially the dual production of IFNγ
333 and TNFα compared to PBS, IT *Lm* only, or IV *Lm* only (**Figure 5D**).
334 To test whether $CD4^+$, $CD8^+$, or both populations of T cells were required for
335 tumor control, we used antibody-mediated depletion of the T cells beginning one day
336 prior to IT *Lm* injection **(Figure 5E)**. Depletion of CD8 T cells abrogated the efficacy of
337 the IV+IT *Lm* regimen in MC38 and B16F10 models, indicating that CD8 T cells were
338 required for tumor control with IV+IT *Lm* **(Figure 5F and Figure S5E-5F)**. In addition,
339 CD8 T cell depletion increased the frequency of $Ly6G^+$ cells maintained in tumors of
340 mice treated with IV+IT *Lm*, suggesting that the reduction in PMN-MDSCs with IV+IT
341 *Lm* is likely the result of CD8 T cell killing of *Lm*-infected PMNs (**Figure 5G**). We also
342 tested the IV+IT dosing regimen in *Batf3*$^{-/-}$ mice that lack type I dendritic cells (DC1s),
343 which are the primary DCs responsible for cross-presenting *Listeria* antigens to CD8 T
344 cells[73,74]. The IV+IT dosing regimen did not lead to tumor control in *Batf3*$^{-/-}$ mice **(Figure**
345 **5H and Figure S5G)**. Taken together, the above results suggested that IV+IT *Lm*
346 therapy requires the activity of T cells, in particular CD8 T cells. However, whether CD8
347 T cells specific to *Listeria*, the tumor, or both were required for tumor control could not
348 be distinguished.
349

350 ***Listeria*-specific CD8 T cells drive tumor control.**
351 To assess whether the CD8 T cells that mediate tumor control with IV+IT *Lm*
352 treatment are specific to *Lm* antigens, we used *Lm* engineered to express ovalbumin
353 (*Lm-OVA*) and MHC-I (H2-K^b) tetramers loaded with SIINFEKL to track the anti-*Lm*
354 response (SIIN/H2K^b) (**Figures 6A** and **S6A**). We observed an increased frequency of
355 SIIN/H2K^b CD8 T cells in tumors with IV alone and IV+IT *Lm*, but only a significant
356 increase in the absolute number of these *Lm*-specific cells in tumors with IV+IT *Lm*
357 (**Figure 6A**). To test whether anti-*Lm* CD8 T cells alone could replace IV *Lm*
358 administration to mediate tumor control, we used CD8 T cells from OT-I mice, which
359 have a TCR that recognizes the OVA peptide SIINFEKL presented on MHC I
360 (SIIN/H2K^b). Adoptive transfer of activated OT-I CD8 T cells into mice prior to tumor
361 inoculation allowed for a pool of *Lm*(SIIN)-specific memory CD8 T cells to develop in
362 recipient mice, analogous to the expansion of *Lm*-specific memory CD8 T cells in
363 prophylactically IV *Lm*-treated mice (**Figure 4G-H**). When tumors became palpable at
364 day 11, tumors were injected with PBS, *Lm*, or *Lm-OVA* (**Figure 6B**). Strikingly, only
365 mice whose tumors were injected with *Lm-OVA* had delayed tumor growth, similar to
366 mice that received a standard IV+IT *Lm* regimen (**Figurse 6B** and **S6B**). Even in the
367 aggressive orthotopic KP sarcoma model that does not express tumor-specific
368 antigens[75], the transfer of *Lm*-specific CD8 T cells prior to tumor implantation and IT
369 *Lm-OVA* treatment was sufficient to provide significant tumor control (**Figures 6C** and
370 **S6C**). These results indicate that a CD8 T cell response specific to *Lm* antigens is
371 sufficient to phenocopy the effect of IV *Lm* in the IV+IT *Lm* dosing regimen.
372
373 ***Listeria*-specific CD8 T cells control tumors without direct recognition of tumor**
374 **cells.**
375 It has been reported that an alternatively attenuated strain of *Listeria* can directly
376 infect cancer cells, and this could lead to the direct killing of tumor cells by *Listeria*-
377 specific CD8 T cells[76]. While we did not find evidence of *Lm* infecting tumor cells using
378 the *Lm-RFP* reporter strain **(Figures 2A-2D**), we wanted to test whether direct tumor
379 cell killing by *Lm*-specific CD8 T cells was required for tumor control. To do this, we
380 again transferred OT-I CD8 T cells prior to tumor development, but now tested their
381 efficacy against *B2m*$^{-/-}$ (MHC I-deficient) MC38 tumors in either wildtype or *B2m*$^{-/-}$ mice,
382 which lack MHC-I on all host cells (**Figure 6D and Figure S6D**). In this scenario, we
383 could determine whether tumor control with IV+IT *Lm* required the recognition of
384 infected tumor cells or host cells directly by OVA-specific CD8 T cells. In response to
385 MC38-*B2m*$^{-/-}$ tumors, OT-I T cells mediated tumor control with IT *Lm-OVA*, but this only
386 occurred in the setting of wildtype mice and not *B2m*$^{-/-}$ mice (**Figure 6D**). In the setting
387 of wildtype MC38 tumors, MHC-I expression was required on host cells to mediate
388 tumor control, as IT *Lm-OVA* was completely ineffective in *B2m*$^{-/-}$ mice despite the
389 presence of OT-I T cells and MHC I expression on the tumor cells (**Figures 6D and**

390 **S6E**). Furthermore, CFU analysis for live *Lm* also demonstrated that MHC I expression
391 on host cells, but not tumor cells, was absolutely required for *Lm* clearance from the
392 TME, in line with *Lm* persisting in host immune cells rather than tumor cells (**Figure**
393 **S6F**). Thus, *Lm*-specific CD8 T cells require MHC I expression on host cells, but not
394 tumor cells, to control tumors and bacterial load with the IV+IT *Lm* regimen.
395 To test whether the anti-*Lm* CD8 T cells alone were able to mediate tumor
396 control, we injected *in vitro* activated OT-I cells into *Rag2*-deficient mice, which lack T
397 and B cells and therefore cannot mount a direct antitumor CD8 T cell response. We
398 then implanted MC38 tumors and IT injected PBS, *Lm* or *Lm-OVA* at day 11 when
399 tumors became palpable. Here, tumor growth was still significantly reduced in *Rag-2*$^{-/-}$
400 mice that were IT injected with *Lm-OVA*, but not when injected with *Lm* that did not
401 express OVA (**Figures 6E and Figure S6G**). Thus, tumor control could be mediated
402 directly by anti-*Lm* CD8 T cells in the TME in the absence of additional host T cells.
403 To rule out a role for OT-I transgenic T cells and the recognition of OVA antigen
404 in mediating tumor control, we also performed the standard IV+IT *Lm* regimen against
405 MC38-*B2m*$^{-/-}$ tumors and still observed tumor control that did not require MHC I
406 expression on the tumor cells (**Figure 6F and Figure S6H**). Furthermore, the lack of
407 MHC I on tumor cells did not incite NK cell-mediated tumor control in response to
408 missing self because IV+IT *Lm* controlled tumors equivalently with or without anti-NK1.1
409 depletion (**Figure 6F and Figure S6H**). Finally, we tested whether the transfer of T cells
410 specific to natural *Lm* antigens could also drive tumor control by immunizing mice with
411 *Lm*, expanding T cells from these mice *in vitro* with heat-killed *Lm*, and then
412 prophylactically transferring bulk *Lm*-specific CD4 and CD8 T cells instead of OT-I T
413 cells into *Rag2*-deficient mice. Here again, natural *Lm* antigen-specific T cells were able
414 to control tumors in the absence of host T cells (**Figure 6G and Figure S6I**). Overall,
415 these results indicate that T cells specific for *Lm* antigens that recognize non-tumor cells
416 in the TME can mediate significant tumor control.
417
418 ***Listeria*-specific CD8 T cell killing and cytokine production drive tumor control.**
419 Next, we sought to determine how *Lm*-specific CD8 T cells, which do not target
420 the cancer cells directly, mediate tumor control. First, we tested whether killing of non-
421 tumor cells infected with *Lm* was required for the efficacy of the IV+IT *Lm* regimen by
422 prophylactically transferring activated SIIN-specific CD8 T cells generated from WT
423 versus *Prf1*-deficient (*Prf1*$^{-/-}$) mice vaccinated with *Lm-OVA*. Mice were then inoculated
424 with MC38 tumors, and at day 11 (when tumors were palpable), tumors were IT injected
425 with *Lm* or *Lm-OVA* (**Figure 7A**). Tumor control was completely abolished when the
426 transferred *Lm*-specific T cells lacked the pore-forming effector protein Perforin (**Figure**
427 **7B and Figure S7B**). Next, *Lm*-specific T cells that lacked the capacity to secrete IFN-γ
428 (by harvesting SIIN-specific CD8 T cells generated from WT versus *Ifng*$^{-/-}$ mice
429 vaccinated with *Lm-OVA*) also did not mediate tumor control (**Figure 7B and and**

430 **Figure S7A**). Notably, the failure of *Prf1*$^{-/-}$ and *Ifng*$^{-/-}$ SIIN-specific CD8 T cells to
431 mediate tumor control was not due to a failure of these cells to infiltrate the tumors, as
432 an equivalent frequency of SIIN-specific CD8 T cells were found in tumors that received
433 *WT*, *Prf1*$^{-/-}$, or *Ifng*$^{-/-}$ SIIN-specific CD8 T cells (**Figure S7C)**. Since IV+IT *Lm* increased
434 the production of IFN-γ and TNF-α from intratumoral CD8 T cells, we also tested
435 whether secretion of TNF-α was required for the IV+IT *Lm* efficacy by using anti-TNF-α
436 blocking antibodies. TNF-α blockade prevented tumor control with IV+IT *Lm* (**Figure 7C**
437 **and Figure S7D**). Taken together, these results show that both the killing activity and
438 cytokine production of *Lm*-specific CD8 T cells were required to mediate tumor control
439 in the IV+IT *Lm* treatment regimen.
440
441 ***Listeria*-specific CD8 T cells enhance antitumor CD8 T cell responses.**
442 To determine how the IV+IT *Lm* regimen controlled tumors, we performed
443 immunofluorescence analysis on tumors one and ten days after IT *Lm* (with prior IV *Lm*)
444 or IT PBS (with prior IV PBS). We used anti-cleaved caspase 3 (CC3) staining to
445 monitor the induction of apoptosis, as the requirement for Perforin in anti-*Lm* CD8 T
446 cells indicated an important killing activity for the effectiveness of IV+IT *Lm* (**Figure 7B**).
447 Indeed, the IV+IT *Lm* regimen induced a large amount of CC3 staining throughout the
448 tumors one day after IT *Lm* injection, and this increased CC3 staining was markedly
449 reduced by depleting CD8 T cells prior to IT injection (**Figure 7D**). The increase in CC3
450 staining was transient, however, as no differences were noted ten days after IT *Lm*
451 injection (**Figure S7E**). In addition to their potential role in promoting cell killing, the
452 requirement for IFN-γ and TNF-α may also be to slow tumor cell proliferation directly[77].
453 We used anti-phospho-histone H3 (PHH3) staining to monitor tumor cells in mitosis as a
454 marker of cell proliferation and observed a nearly complete loss of PHH3 staining in
455 tumor cells after IV+IT *Lm*, indicative of a near complete inhibition of cell cycle
456 progression (**Figure 7E**). Notably, this reduced proliferation was still observed ten days
457 after IT injection, though less robustly (**Figure S7E**). Thus, increased apoptosis and
458 reduced cell proliferation likely contribute to the elimination and reduced growth of IV+IT
459 *Lm*-treated tumors.
460 The massive induction of cell death upon IV+IT *Lm* may increase the
461 phenomenon of epitope spreading, wherein death of tumor cells leads to the increased
462 release and presentation of tumor antigens[78,79]. Thus, IV+IT *Lm*, while effective in
463 controlling tumor progression with *Lm*-specific CD8 T cells alone, may also enhance the
464 host T cell response directly against tumors. Notably, tumor control with IV+IT *Lm* was
465 better in WT compared to *Rag-2*$^{-/-}$ mice, suggesting that host tumor-specific T cells may
466 contribute to the efficacy of IV+IT Lm. (**Figures 6B versus 6E**). To assess the tumor-
467 specific CD8 T cell response with IV+IT *Lm*, we used MHC I tetramers loaded with a
468 tumor-derived peptide from the endogenous Murine Leukemia retrovirus, p15E (**Figure**
469 **S7F)**[71,72]. Interestingly, while there was a decrease in the frequency and number of

470 tumor-reactive (MuLV/H2K^b tetramer$^+$) CD8 T cells in mice receiving the IV+IT *Lm-OVA*
471 compared to PBS treated mice 8 days after IT injections, the frequency and number of
472 these tumor-specific CD8 T cells was significantly increased compared to mice that only
473 received IV *Lm-OVA* (**Figure 7F**). Furthermore, at later time points after IT injection (20
474 days), the tumor-specific T cells exhibited a phenotype of reduced T cell exhaustion
475 (reduced PD1$^+$Lag-3$^+$ double and single positive cells) (**Figures 7G and S7G**). Thus,
476 while IV *Lm* reduces tumor-specific T cell frequency and numbers, tumor-specific T cells
477 are recalled to tumors following IV+IT *Lm* and retain a less exhausted phenotype
478 throughout tumor growth.
479 Next we tested the importance of cross-presentation by type I dendritic cells
480 (DC1), as we hypothesized that if anti-*Lm* CD8 T cells promoted tumor-specific CD8 T
481 cell control, this would be dependent on DC1 tumor antigen cross-presentation[80,81]. We
482 already observed that IV+IT *Lm* tumor control was completely abrogated in *Batf3$^{-/-}$* mice
483 (**Figure 5H**), likely due to the inability of mice to mount an anti-*Lm* CD8 T cell response
484 after IV *Lm*[74,82]. Therefore, we used the transfer of activated OT-I CD8 T cells into *Batf3^{-}*
485 *$^{/-}$* mice and then only IT injected *Lm* or *Lm-OVA*. We reasoned that this would establish
486 whether cross-presentation after IT *Lm* was required to enhance that antitumor CD8 T
487 cell response and increase tumor control. First, tumor control was only observed with IT
488 *Lm-OVA* and not *Lm* as observed previously. As might be expected, *Batf3$^{-/-}$* mice had
489 significantly reduced tumor control compared to *Batf3$^{+/+}$* mice with IT *Lm-OVA* **(Figure**
490 **7H and S7H)**. However, *Batf3$^{-/-}$* mice treated with IT *Lm-OVA* also had significantly
491 better tumor control than *Batf3$^{-/-}$* mice treated with IT *Lm*, indicating that the OT-I CD8 T
492 cells targeting *Lm* provided significant tumor control in the absence of DC1s (**Figures**
493 **5H versus 7H and S7H**). Most importantly, the frequency of tumor-specific (MuLV/H2K^b
494 tetramer$^+$) CD8 T cells was significantly increased in IT *Lm-OVA*- compared to IT *Lm*-
495 treated mice, and this increase was totally dependent on the presence of Baft3$^+$ DC1s in
496 mice (**Figure 7I**). Finally, using a method we have employed previously to look directly
497 at tumor antigen cross presentation on DC1s using OVA-expressing tumor cells and the
498 25D1.16 monoclonal antibody that detects SIINFEKL peptide from OVA presented on
499 MHC I (H2-K^b)[17,34–36], we observed increased cross-presented tumor antigen on DC1s
500 only with IV+IT *Lm*, but not with IV or IT only *Lm* administrations (**Figure 7J**). These
501 results support the hypothesis that the *Lm*-specific CD8 T cells are able to enhance the
502 tumor-specific CD8 T cell response by promoting the cross presentation of tumor
503 antigens on Batf3$^+$ DC1s, which may be particularly important for sustained control of
504 tumors at later time points.
505 To directly test whether antitumor CD8 T cells also play a role in tumor control in
506 our IV+IT *Lm* dosing regimen, we monitored tumor growth in the presence or absence
507 of host T cells in the context of adoptive OT-1 T cell transfer to surrogate *Lm*-specific
508 CD8 T cells. To do this, we generated a T cell depleter mouse model by combining
509 *CD4-Cre* and *R26$^{LSL-DTR}$* alleles[82]. Because all host T cells upregulate CD4 during

510 thymic development, both mature CD4 and CD8 T cells permanently express the
511 diphtheria toxin receptor and are depleted with the addition of diphtheria toxin (DT)
512 (**Figure S7I)**[83]. Into these mice, we adoptively transferred *in vitro* activated OT-I CD8 T
513 cells, transplanted MC38 tumors two weeks later, and then began DT treatment one day
514 prior to IT injection of *Lm* or *Lm-OVA*. In the setting of tumor control with IT *Lm-OVA*, we
515 now observed that the depletion of host T cells by DT treatment in *CD4-Cre*$^+$ (host T
516 cells depleted) compared to *CD4-Cre*$^-$ (host T cells not depleted) mice significantly
517 reduced tumor control *(***Figures 7K and S7J)**. However, as expected, mice were still
518 able to significantly control tumors without host T cells when treated with *IT Lm-OVA*
519 compared to IT *Lm* (comparing *CD4-Cre*$^+$ mouse groups), indicating that *Lm*-specific
520 OT-I CD8 T cells alone do provide significant tumor control (**Figures 7K and S7K**).
521 Altogether, these data demonstrate that, in addition to *Lm*-specific CD8 T cells
522 controlling tumors directly, they also enhance the tumor-specific CD8 T cell response by
523 promoting the expansion and function of these CD8 T cells to increase tumor control.
524
525 **Discussion:**
526 In this study, we report two major findings. First, we showed that direct
527 intratumoral injection of an attenuated strain of *Lm* caused increased tumor growth. This
528 was due to *Lm*-mediated recruitment of PMNs that are converted within tumors into
529 immunosuppressive MDSCs, which act as permissive cells for bacterial survival while
530 also suppressing antitumor CD8 T cells. Second, we showed that IT *Lm* tumor growth
531 promotion could be converted to tumor control by prior IV *Lm* immunization, which
532 generated anti-*Listeria* CD8 T cells whose activity alone could mediate cancer
533 protection. Thus, depending on the context of intratumoral seeding of *Lm* into a tumor,
534 *Listeria* can either promote or inhibit cancer progression. These results reveal new
535 insights into the biology of *Listeria* colonization of tumors in immune competent mice as
536 well as the potential for anti-*Lm*-specific CD8 T cells to contribute to cancer control.
537 These findings redefine the therapeutic mechanisms of action of bacterial cancer
538 therapy and reveal the potential of immunological targeting of bacteria that colonize
539 tumors to treat cancer.
540 The *ΔactA* attenuated *Lm* strain used in this study selectively colonized and
541 persisted in tumors when injected IT or IV. Other studies have also reported short-term
542 persistence of bacteria in tumors, either growing intracellularly (e.g. *Salmonella*) and/or
543 extracellularly (e.g. *Clostridium*, *Vibrio. cholerae*, *E. coli)*, which in some cases had
544 direct tumoricidal effects[5,84,85]. *Clostridium novyi* administered intravenously led to
545 sporulation in the avascular regions of tumors that directly caused cancer cell death[13,86].
546 Longer term protection from cancer with *Clostridium* occurred in ~30% of mice and
547 depended on the generation of CD8 T cells, though the specificity of the CD8 T cells,
548 against bacteria or tumor, was never directly tested[13,86]*. E. coli* engineered to express
549 tumor antigens, the pore forming protein α-hemolysin, or L-arginine to promote CD8 T

550 cell function, both led to improved tumor control upon bacterial colonization of
551 tumors[21,87,88]. The prevalence of bacteria in tumors has been attributed to the presence
552 of nutrients or an environment in tumors that is conducive to bacterial survival and
553 growth[12,13,89–91]. *Salmonella typhimurium* engineered to infiltrate tumors by selective
554 auxotrophy was effective at controlling several types of mouse tumors[12,89,92]. The lack of
555 documentation of *Lm* persistence in tumors could be the result of using alternative
556 attenuated strains of *Listeria* or failing to look for *Lm* persistence in previous studies.
557 However, in the case of *ΔactA*-attenuated *Listeria* colonization in this study, we
558 hypothesize that bacterial migration via the bloodstream is stochastic, but upon arrival in
559 tumors, *Listeria* is protected from immune clearance due to the immunosuppressive
560 environment created in tumors that generates PMN-MDSCs that permit the intracellular
561 growth of *Lm*[5,93].
562 PMN permissiveness for cytosolic *Lm* was strongly correlated with a CD14$^+$ and
563 PD-L1$^+$ phenotype of the PMNs, markers associated with a MDSC phenotype. We also
564 found that this phenotype was promoted by tumor derived factors, since culture of
565 PMNs with tumor cell supernatants was sufficient to induce their expression of CD14
566 and PD-L1. In our system, however, depletion of these PMN-MDSCs did not prevent *Lm*
567 persistence in tumors, but did prevent the accelerated tumor growth observed with IT
568 *Lm* alone. This suggests that the TME prevents *Lm* clearance in multiple phagocytic
569 immune cell types, but that recruitment and conversion of PMNs to MDSCs specifically
570 promotes cancer progression. PMN-MDSCs and other myeloid cells have been found to
571 promote tumor growth by several mechanisms, such as inhibiting T cell responses as
572 well as by promoting vasculature formation to support tumor cell proliferation in
573 glioblastoma, pancreatic, and several other mouse tumor models[35,38,64]. Using *in vitro*
574 co-culture of FACS-purified intratumoral PMN-MDSCs with tumor cells and antitumor
575 CD8 T cells, we showed that PMN-MDSCs could inhibit cytokine production from CD8 T
576 cells responding to antigen recognition on tumor cells. Altogether, we uncovered an
577 unexpected consequence of *Lm* seeding and colonization of tumors, wherein bacterial
578 colonization of tumors by *Lm* does not lead to direct tumoricidal effects, but rather,
579 recruits immune cells that are subsequently converted into immunosuppressive cells
580 that promote tumor growth. However, microbes have also been shown to directly
581 promote immune tolerance, and so it is possible that *Lm* directly promotes tolerance in
582 the TME and its clearance with the IV+IT regimen allows for stronger tumor control[94].
583 Attenuated *Listeria* vaccines generate memory CD8 and CD4 T cells that
584 provide robust and long-lasting adaptive immunity[24,65]. We tested whether prior IV *Lm*
585 administration to generate anti-*Lm* CD8 T cells would impact the immunosuppressive
586 TME and promote tumor control with a secondary IT *Lm* dose. In this setting, IT *Lm* led
587 to tumor control across multiple tumor models, including an aggressive orthotopic KP
588 model of sarcoma. Tumor control was also observed if mice were prophylactically
589 vaccinated prior to tumor inoculation, ruling out a role for tumor colonization with IV *Lm*

590 in the efficacy of this IV+IT *Lm* regimen. Our results parallel previous approaches taking
591 advantage of TDAP vaccination and using *Listeria* as a delivery system to introduce
592 tetanus toxoid into tumors to elicit a $CD4^+$ memory T cell response to eliminate tumor
593 cells[76]. However, unlike that study, we found a clear requirement for CD8 T cells in
594 mediating tumor control. Furthermore, in prior reports, it was shown that the *Listeria*
595 infected the cancer cells directly to drive T cell recognition and control of cancer[76].
596 However, in our study we used a RFP reporter to identify cytosolic *Lm* and did not find
597 evidence of direct infection of tumor cells. Nor was direct recognition of tumor cells by
598 anti-*Lm* CD8 T cells required for tumor control, as MHC-I-deficient (*B2m*$^{-/-}$) tumors were
599 also controlled by the OT-I+IT *Lm-OVA* or the IV+IT *Lm* regimen. Furthermore, control
600 of MHC-I-deficient tumors was not mediated by NK cells. However, MHC-I expression
601 on non-tumor cells was essential for tumor control, as *B2m*-deficient mice receiving anti-
602 *Lm* OT-I T cells were unable to control tumors after IT *Lm-OVA* administration.
603 Therefore, CD8 T cell recognition of host cells, presumably $CD45^+$ immune cells that
604 have taken up *Lm* in their cytosol, including PMN-MDSCs, was required for tumor
605 control. The differences in mechanisms across studies could be the result of differences
606 in the attenuated strains of *Listeria* used. Our study used an *ΔactA* mutation to
607 attenuate the bacteria and prevent cell to cell spread, whereas others have used
608 alternatively attenuated *Listeria* that retains a functional *actA* gene, thus allowing for the
609 spread of *Listeria* to non-phagocytic cells, including tumor cells[17–20,23,76,91,95]. Overall,
610 while direct tumor cell infection may support immune responses to tumors, our results
611 indicate that tumor control by CD8 T cells does not necessitate bacterial spread into
612 tumor cells.
613 To test the specificity of the CD8 T cells required for tumor control with IT *Lm*, we
614 first tested the importance of anti-*Lm*-specific CD8 T cells by adoptive transfer of TCR
615 transgenic (OT-I) CD8 T cells or polyclonal natural *Lm* antigen-specific T cells in place
616 of IV *Lm* administration. We then used *Lm* IT delivery to show that T cells targeting *Lm*
617 antigens, which were incapable of recognizing tumor antigens, could mediate tumor
618 control. Tumor control with *Lm*-specific T cells even occurred after transfer into *Rag-2*$^{-/-}$
619 mice that could not generate any tumor-specific T cell responses, showing clearly that
620 bacteria-directed T cells responding within the TME can control cancer. These results
621 are contrary to the established dogma that an increase in tumor-specific CD8 T cells is
622 required for the efficacy of bacterial-based cancer immunotherapies[96]. Of note, in
623 clinical trials using BCG treatment for bladder cancer, patients with a positive skin
624 tuberculosis test (PPD) due to previous vaccination with BCG, responded better to the
625 BCG treatment and had longer recurrence-free survival than patients who did not
626 establish pre-existing BCG-specific T cell immunity[97].
627 To identify the functionalities of anti-*Lm* CD8 T cells required for tumor control,
628 we transferred *Lm*-specific *Prf1*$^{-/-}$ or *Ifng*$^{-/-}$ CD8 T cells or used TNF-α blockade to show
629 that killing activity, as well as IFN-γ and TNF-α production, were required for tumor

630 control. We hypothesize that killing activity by CD8 T cells is required to eliminate PMN-
631 MDSCs and the *Listeria* residing within them. This was evidenced by a high level of
632 CC3-staining one day after IT *Lm* delivery exclusively in the IV+IT *Lm*-treated tumors
633 that was dependent on CD8 T cells. IFN-γ and TNF-α production may be necessary to
634 induce MHC I expression on these cells to mediate robust killing of *Lm*-infected cells,
635 and/or it may act directly on tumor cells to reduce tumor cell proliferation[98–100]. In line
636 with this, we observed a marked reduction in $PHH3^{+}$ tumor cells with IV+IT *Lm*
637 immediately following IT *Lm* delivery at one day and a sustained reduction in tumor cell
638 proliferation for up to 10 days afterwards that was also dependent on CD8 T cells.
639 Finally, and perhaps most interestingly, IV+IT *Lm* enhanced the accessibility to
640 tumor-derived antigens for cross presentation by cDC1s to tumor-specific CD8 T cells
641 by an antigen spreading phenomenon[101–103]. This was evidenced by both increased
642 tumor antigen presentation on DC1s and increased tumor-specific CD8 T cells
643 infiltrating tumors with IV+IT *Lm* compared to IV *Lm* alone. In addition, tumor-specific
644 CD8 T cells were less exhausted. We confirmed the importance of DC1s and tumor-
645 specific T cells by genetic deficiency for DC1s (*Batf-3*$^{-/-}$) or tumor-specific T cells (*CD4-*
646 *Cre;R26*$^{LSL\text{-}DTR}$, T depleter) and showing significant loss of tumor control in either
647 scenario. However, the activity of anti-*Listeria* CD8 T cells were still paramount to tumor
648 control, as their depletion completely restored rapid tumor growth. Thus, the anti-*Listeria*
649 T cell response not only controls tumors indirectly, by promoting strong, localized cell
650 death in the tumor and inhibiting tumor proliferation, but these activities also increase
651 epitope spreading of tumor antigens, enhancing the tumor-specific CD8 T cell response
652 to provide long-lasting systemic tumor immunity.
653 In conclusion, we have shown bacterial immunotherapy can have unintended
654 negative outcomes by driving the accumulation of immunosuppressive cell types within
655 tumors. However, the tumor promoting impact of *Lm* can be overcome by using a *Lm*
656 dosing regimen that first generates anti-*Lm* CD8 T cells before direct intratumoral
657 administration. The CD8 T cell response against *Lm* can not only remove the
658 immunosuppressive cells from tumors, but also through direct cell killing of non-tumor
659 cells in the TME, promote tumor control. Because the T cell responses against certain
660 pathogens (i.e. *Listeria*, BCG, influenza, etc.) have been heavily studied and
661 characterized, these findings have far-reaching consequences and may reveal new
662 applications for existing therapeutics and vaccines. In addition, we show that methods
663 to expand pathogen-specific T cells *ex vivo* for adoptive transfer of bacterial or viral
664 antigen-specific T cells are effective and may be safer than attempting to generate
665 memory T cells by active vaccination in potentially immunocompromised individuals, like
666 cancer patients[104]. Collectively, our study demonstrates new insights into the
667 inefficiencies of current bacterial immunotherapy approaches and reveals a tumor
668 antigen-free, bacterial-based dosing regimen that can control cancer independently of
669 its immunogenicity or the identification of tumor neoantigens. Most importantly, the

recent findings that many tumors are colonized by various bacterial species opens the door to a new alternative strategy to modify the tumor microenvironment and treat cancer, by targeting intratumoral bacteria.

Limitations of the study:

This study only used one attenuated strain of *Listeria monocytogenes* for all investigations and while we hypothesize that the findings will be generalizable to other bacterial species, or even other attenuated strains of *Listeria*, this remains to be tested. Future studies will also need to test what specific bacterial attributes of *Listeria* are required to promote tumor control - such as the capacity for intracellular invasion or the capacity to activate specific innate pattern recognition receptors, which will shed light on the broad applicability of these findings to other bacterial species. Next, while we showed that *Lm* colonization of a non-subcutaneous tumor model (PDAC) also occurred, further investigations to test whether the IV+IT (or IV+IV) *Lm* therapeutic strategy is also effective against internally arising epithelial cancers need to be performed. Finally, the findings here rely solely on mouse cancer models. Future studies should examine whether human tumors will yield similar results, such as with humanized mouse models or the examination of human tumor samples, especially from patients who have been treated with *Listeria* vaccines.

Acknowledgments:

We thank Russell Vance, Gregory Barton, David Raulet, and Thomas Dubensky for reviewing the manuscript and providing feedback; Hector Nolla, Alma Valleros, Kartoosh Heydari and Anita Wong Lin of the UC Berkeley Cancer Research Laboratory Flow Cytometry Facility. This research was supported by 1DP2CA247830-01 from the National Institutes of Health (NCI) and C23CR5612 from the UC CRCC Cancer Research Coordinating Committee. M.D. is a Pew-Stewart Scholar and a St. Baldrick's Scholar with generous support from Hope with Hazel. J.G.C is a HHMI Gilliam Fellow.

Author Contributions:

Conceptualization and Methodology, M.D., D.A.P., J.G.C., S.F., T.F.C; Investigation, J.G.C., S.F., T.F.C., J.W., D.G.V., J.Y., N.F.H., E.W., and M.D.; Writing – Original Draft, M.D., J.G.C., S.F.; Writing – Review & Editing, M.D., D.A.P., J.G.C., S.F., T.F.C; Supervision, M.D., D.A.P., J.G.C., S.F.; Funding Acquisition, M.D., D.A.P.

Declaration of Interests:

D.A.P. is on the board of directors for Laguna Therapeutics.

STAR Methods:

Resource Availability

710 **Lead Contact**
711
712 Further information and requests for resources and reagents should be directed to and
713 will be fulfilled by the lead contact, Michel DuPage (dupage@berkeley.edu).
714
715 **Materials availability**
716 *Listeria* monocytogenes strains used in the study will be made available from the lead
717 contact upon request.
718
719 **Data and code availability**
720 Any additional information required to reanalyze the data reported in this paper is
721 available from the lead contact upon request.
722
723 **Experimental models and subject details:**
724 **Animal studies**
725 C57BL/6J wildtype mice were obtained from Jackson laboratories (JAX:000664) and
726 bred in house. OT-1 transgenic mice were obtained Taconic (Catalog#: 2334) and bred
727 in house. Prf1$^{-/-}$ mice were a gift from the Stanley lab at the University of California,
728 Berkeley (JAX:000274). Rag2$^{-/-}$ (JAX:008449) and β*2m2m*$^{-/-}$ (JAX:002087) mice were a
729 gift from the Raulet lab at the University of California, Berkeley. CD4^{Cre} mice were
730 obtained from Jackson laboratories (JAX:022071) and bred in house. R26^{DTR} mice were
731 obtained from Jackson laboratories (JAX:008040) and bred in house. Sarcoma cell lines
732 were generated in *Kras*$^{LSL\text{-}G12D/+}$*;p53*$^{fl/fl}$ *mice* by intramuscular injection of the left hind
733 limb with replication-incompetent lentiviruses expressing Cre recombinase as reported
734 previously, harvested, and cultured[75]. For tumor studies, syngeneic C57BL/6J mice
735 were inoculated with 5.0x10^5 MC38 or 2.0x10^5 B16F10 cells in PBS subcutaneously. KP
736 sarcoma cells were inoculated into C57BL/6J mice with 5.0x10^5 cells by intramuscular
737 injection of the right hind limb. For diphtheria toxin (DT) treatment for T cell depletions,
738 we injected 1µg every 2 days by i.p. Tumor measurements were performed blindly
739 across the entire experiment by a single operator measuring three dimensions of the
740 tumor with calipers three times per week. All the experiments were conducted according
741 to the Institutional Animal Care and Use Committee guidelines of the University of
742 California, Berkeley.
743
744 **Cell lines**
745 MC38 and B16F10 cell lines were kindly provided by Dr. Jeff Bluestone's lab[105]. MC38-
746 β2m$^{-/-}$ cell line was kindly provided by Dr. David Raulet's lab[47]. All cell lines were
747 maintained in DMEM (GIBCO) supplemented with 10% FBS, sodium pyruvate (GIBCO),
748 10mM HEPES (GIBCO), and penicillin-streptomycin (GIBCO). Tumor cells were grown
749 at 37℃ with 5% CO_2.

750
751 **Method Details:**
752 ***Listeria monocytogenes* strains**
753 All strains of *L. monocytogenes* were derived from the wild-type 10403S strain. The *Lm*
754 constructs were based on an attenuating deletion of the actA gene (*ΔactA*). *Lm-OVA*
755 expresses an LLO-OVA fusion encompassing amino acids 1-441 of Listeriolysin O
756 (LLO) and OVA cloned in frame of LLO1-441 under the control of the LLO promoter in
757 the pPL2 integration vector[106]. *Lm-TagRFP* expresses a secreted TagRFP protein
758 under the control of the *actA* promoter using the pPL2 integration vector[52]. All strains
759 were cultured in filter-sterilized nutrient-rich Brain Heart Infusion (BHI) media (BD
760 Biosciences) containing 200 µg/mL streptomycin (Sigma-Aldrich).
761
762 **Intravenous and Intratumoral *Listeria* infection**
763 Overnight cultures were grown in BHI + 200 µg/mL streptomycin at 30℃. The following
764 day, bacteria were grown to logarithmic phase by diluting the overnight culture in fresh
765 BHI + 200 µg/mL streptomycin and culturing at 37℃ shaking. Log-phase bacteria were
766 washed and frozen in 9% glycerol/PBS. For intravenous infections, frozen stocks were
767 diluted in PBS to infect via the tail vein with 1 x 10^6 CFU log-phase bacteria. For
768 intravenous infections, frozen stocks were diluted in PBS to infect via intratumoral
769 infections at 5 x 10^7 CFU log-phase bacteria. The mice were euthanized 8-20 days after
770 intratumoral injections and organs were collected for flow analysis.
771
772 **Colony forming unit assays from tissues**
773 Tissues were collected in 0.1% NP40 buffer diluted in PBS. Organs were homogenized
774 and serially diluted on non-TC treated 96-well plates (Genesee). Serial dilutions were
775 plated on BHI + 200 µg/mL streptomycin plates. Plates were incubated overnight at
776 37℃.
777
778 **CIN/Primary bone-marrow derived PMN Maintenance and Differentiation:**
779 Cas9+ ER-Hoxb8 conditionally immortalized neutrophils (CINs) were a gift from the
780 Stanley lab at the University of California, Berkeley[61]. CINs were expanded as
781 progenitors in Optimem with 10% FBS, 1% L-glutamine, 30µM 2-mercaptoethanol, and
782 1% Stem-cell factor (SCF)-producing CHO cell supernatant (CIN Media) that also
783 contained 1µM beta-estradiol in non-TC treated flasks (Genesee) maintaining a
784 concentration less than 1x10^6 cells/mL. Upon reaching the desired quantity, non-
785 adherent progenitors were harvested, washed twice in cold PBS 1x, and plated in non-
786 TC treated flasks containing CIN media lacking beta-estradiol. To generate PMNs, CINs
787 were differentiated until Day 6 in CIN Media + 5ng/mL GM-CSF. To generate PMN-
788 MDSCs, CINs were differentiated in CIN media + 5ng/mL GM-CSF, 40ng/mL IL-6, and
789 40ng/mL GM-CSF. For primary bone marrow PMNs and PMN-MDSCs, cells were

790 isolated and cultured as described[63]. To generate PMNs-MDSCs, cells were cultured in
791 40ng/mL IL-6 and 40ng/mL GM-CSF1 day post isolation for 6 days.
792
793 **In vitro infections:**
794 Cells were infected with *Lm-TagRFP* at an MOI that resulted in 30% of the cells being
795 infected. At 1hr post infection, 50µg/mL Gentamicin was added to kill all extracellular
796 Listeria. For flow analysis, cells were collected at time points indicated, stained, and
797 fixed with 4% PFA.
798
799 **Cancer Supernatant Assays**
800 Cancer cell supernatant was generated via the expansion of MC38, B16F10, and 3T3
801 cell lines in TC-treated flasks in Optimem + 10% FBS, followed by collection of
802 supernatant fluid when cells reached near ~100% confluency. After filtration, all
803 supernatants were frozen down at -20°C. Surveying cancer supernatants involved a 24h
804 incubation period where cells were either re-seeded into TC-treated 24 well plates or
805 non-TC treated flasks in fresh CIN media with a 50:50 ratio of MC38, B16F10, or 3T3
806 supernatant. Cells were collected at 24h, stained, fixed with 4% PFA, and analyzed by
807 flow cytometry.
808
809 **Tissue Collection and preparation for Flow cytometry**
810 Flow cytometry was performed on an BD LSR Fortessa X20 (BD Biosciences), CyTEK
811 Aurora (CyTEK Biosciences) or LSRFortessa (BD Biosciences) and datasets were
812 analyzed using FlowJo software (Tree Star). Single cell suspensions were prepared in
813 ice-cold FACS buffer (PBS with 2mM EDTA and 1% BS) and subjected to red blood cell
814 lysis using ACK buffer (150mM NH4Cl, 10mM KHCO3, 0.1mM Na2EDTA, pH7.3). Dead
815 cells were stained with Live/Dead Fixable Blue or Aqua Dead Cell Stain kit (Molecular
816 Probes) in PBS at 4℃. Cell surface antigens were stained at 4℃ using a mixture of
817 fluorophore-conjugated antibodies. Surface marker stains for murine samples were
818 carried out with anti-mouse CD3 (17A2, BioLegend), anti-mouse CD4 (RM4-5,
819 BioLegend), anti-mouse CD8a (53-6.7, BioLegend), anti-mouse, CD44 (IM7, BioLeged),
820 anti-mouse CD45 (30-F11, BioLegend), anti-H-2Kb MuLV p15E Tetramer-KSPWFTTL
821 (MBL), anti-H-Kb-A2/SIINFEKEL tetramer (NIH tetramer core), anti-
822 IAb/NEKYAQAYPNVS tetramer (NIH tetramer core) in PBS, 0.5% BSA. Cells were
823 fixed using the eBioscience Foxp3/Transcription Factor staining buffer set
824 (eBioscience), prior to intracellular staining. Intracellular staining was performed using
825 anti-mouse Foxp3 (FJK-16S, eBioscience), anti-mouse TNF-α (MP6-XT22, BioLegend),
826 anti-mouse IFN-γ (XMG1.2, eBioscience), at 4℃, according to manufacturer's
827 instructions. For Lm-TagRFP infected tissues, single cell suspensions were prepared as
828 above, stained using a mixture of fluorophore-conjugated antibodies at 4℃, and fixed in
829 4% PFA. Cells analyzed by flow cytometry the following day to prevent signal loss from

830 flourescent protein. Cells were resuspended in PBS and filtered through a 70-µm nylon
831 mesh before data acquisition. Datasets were analyzed using FlowJo software (Tree
832 Star).
833
834 **Restimulation Assays**
835 Resected tumors were minced to 1 mm^3 fragments and digested in RPMI media
836 supplemented with 4-(2-hydroxyethyl)-1-piperazi-neethanesulfonic acid (HEPES), 20
837 mg/mL DNase I (Roche), and 125 U/mL collagenase D (Roche) using an orbital shaker
838 at 37℃. Cells from lymphoid organs were prepared by mechanical disruption pressing
839 against a 70-µm nylon mesh. All the cell suspensions were passed through 40 µm filters
840 before in vitro stimulation. Cytokine staining was performed with 3-5x10^6 cells in Opti-
841 MEM media supplemented with Brefeldin A (eBioscience) or 10 ng/mL phorbol 12-
842 myristate 13-acetate (PMA) (Sigma), and 0.25 µM ionomycin (Sigma).
843 Fixation/permeabilization of cells was conducted for intracellular staining using the
844 eBioscience Foxp3 fixation/permeabilization kit (BioLegend) or Tonbo Foxp3 /
845 Transcription Factor Staining Buffer Kit.
846
847 **Adoptive transfer experiments**
848 For in vitro T cell culture, spleens and lymph nodes were collected from OT-1 transgenic
849 mice or C57BL/6J wildtype (*WT*) or *Prf1*$^{-/-}$ previously vaccinated with 1.0x10^6 CFU *Lm-*
850 *OVA* 3-4 weeks prior. OT-1s or OVA-responsive CD8s were were activated with 1µg/mL
851 SIINFEKL peptide in DMEM medium supplemented with 10% FBS, non-essential amino
852 acids, sodium pyruvate, L-glutamine, HEPES, 55 µM β-ME and 200 IU/ml recombinant
853 human IL-2 (TECIMTM, Hoffman-La Roche provided by NCI repository, Frederick
854 National Laboratory for Cancer Research). T cells were transferred into WT or Rag2$^{-/-}$ or
855 *B2m*$^{-/-}$ mice by intravenous injection two weeks prior to MC38 or KP sarcoma
856 inoculations.
857
858 ***In vivo* antibody-mediated cell depletion**
859 For tumor progression studies, CD8 depletion was achieved by intraperitoneal injection
860 of 200 µg per mouse of the anti-CD8 monoclonal antibody clone YST-169 (Leinco
861 Technologies, Catalog # C2442) two days prior to tumor inoculation, followed by
862 additional doses every 6 days thereafter. For CD4 depletion, intraperitoneal injection of
863 200 µg/mouse of clone GK1.5 (Leinco Technologies, Catalog: C1333) was done two
864 days prior to tumor inoculation, followed by additional doses every 6 days thereafter.
865 PMN depletion was done by intraperitoneal injection of 200 µg per mouse of the anti-
866 Ly6G monoclonal antibody clone IA8 (Leinco Technologies, Catalog: L280) twice prior
867 to tumor inoculation, followed by additional doses every 2 days.
868
869 **Immunofluorescence & Imaging Analysis**

870 Tissue Sections were washed with PBS and blocked with tissue staining buffer plus
871 10% fetal bovine serum. Tissues were then stained with anti-Ly6G Alexa Fluor 488
872 antibody (Clone 1A8, Biolegend Catalog# 127624), anti- Phospho-Histone H3 (Ser10)
873 antibody (Cell Signaling Catalog# 9701S, or anti-Cleaved Caspase-3 (Asp175) antibody
874 (Clone 5A1E, Cell Signaling Catalog# 9664S) O/N at 4℃ in tissue staining buffer (PBS
875 with 0.2% Triton X-100, 2% FBS) and washed with PBS. For sections stained with
876 unconjugated primary antibodies, sections were incubated with Goat anti-Rabbit IgG
877 (H+L) Cross-Adsorbed Secondary Antibody, Alexa Fluor™ 488 (Thermo Fisher
878 Scientific, Catalog# A-11008) for 1 hour at RT followed by washes with PBS. Tissues
879 were stained with Wheat Germ Agglutinin (WGA) Alexa Fluor 647 (Thermo Fisher
880 Scientific, Catalog# W32466) for 45 mins at RT and washed with PBS. Stained tissue
881 sections were mounted with Fluoromount-G Mounting Medium (Southern Biotech).
882 Images were taken using Zeiss LSM 780 NLO microscope and Zeiss Axioscan 7 or
883 Axioscan Z1. Imaging analysis was performed using Zeiss Zen Lite Imaging Software or
884 Fiji/ImageJ. Quantification of phH3 staining was performed by cropping full Axioscan
885 images into 2 mm x 2 mm images from which 3 representative cropped images per
886 tumor were chosen for counting. Individual PHH3+ cells in these sections were blocked
887 out using the Fiji/ImageJ paintbrush tool until no PHH3+ cells remained visible. A click
888 counter (Mousotron) was used to track the number of cells per section.
889
890 **Statistical Methods**
891 p values were obtained from unpaired two-tailed Student's t tests for all statistical
892 comparisons between two groups, and data were displayed as mean ± SEMs. For
893 multiple comparisons, one-way ANOVA was used. For tumor growth curves, two-way
894 ANOVA was used with Sidak's multiple comparisons test performed at each time point
895 or by multiple regression analysis p values are denoted in figures by *$p < 0.05$, **$p <$
896 0.01, ***$p < 0.001$, and ****$p < 0.0001$.
897
898 **Figure Legends**:
899 **Figure 1 | Intratumoral injection of *Lm* leads to increased tumor growth and**
900 **persistent colonization of *Lm* within tumors.**
901 (A) Experimental design.
902 (B-C) C57BL/6J WT mice were injected with $5x10^5$ MC38 (B, data shown from n= 4-5
903 mice per group from one of three experiments) or $2x10^5$ B16F10 (C, data shown from
904 n=4-5 mice per group from one of two experiments) tumor cells and then $5x10^7$ *Lm*
905 CFUs IT 11 days later and tumors measured.

906 (D-E) CFU analysis for *Lm* from indicated tissues after injection IT (D, $5x10^7$ CFU, n=4-8
907 mice pooled from two experiments) or IV (E, $1x10^6$ CFU, n=4-5 mice pooled from two
908 experiments) of *Lm* 11 days after MC38 or B16F10 tumor inoculation. tdLN = tumor-
909 draining lymph node, ndLN = non-tumor-draining LN.
910 (F) CFU analysis for *Lm* at indicated time points from PDAC pancreatic tissue after
911 orthotopic transplantation of FC1245[107](n=4 mice). 10^6 CFU of Lm injected on day 7.
912 For all plots, *P<0.05, **P<0.01 by two-way ANOVA, mean ± s.e.m.
913
914 **Figure 2 | *Lm* localizes in intratumoral PMNs.**
915 (A) Schematic of Tag-RFP expression from *Lm-RFP*.
916 (B) Representative flow plots from single cell suspensions of MC38 tumors 4 hours post
917 IT *Lm* (left) or IT *Lm-RFP* (right) showing CD45 staining versus Tag-RFP fluorescence.
918 (C) Distribution of RFP^+ immune cell types from MC38 tumors at 4 (left) or 24 (right)
919 hours after IT *Lm* (representative data from three experiments with n= 3-6 mice/group).
920 (D) Analysis of the fraction of PMNs and TAMs that were RFP^+ at 1, 3, and 5 days after
921 IT *Lm-RFP* in MC38 tumors (representative data from two experiments with n= 3-6
922 mice/group).
923 (E) Frequency of $Ly6G^+$ PMNs in spleen or tumors from MC38-bearing mice at 4 and 24
924 hours after IT PBS or IT *Lm*.
925 (F) Frequency of intratumoral $Ly6G^+$ cells that were RFP^+ at 4 and 24 hours after IT
926 PBS or IT *Lm*. Results in E-F are pooled from three experiments with n= 2-5 mice/group
927 per experiment.
928 (G) Images of MC38 tumors 4hrs after IT *Lm*: DAPI (blue), *Lm-RFP* (red), Ly6G (green).
929 Scale bar = 20 μm.
930 (H) Schematic for cytospin imaging analysis of sorted intratumoral Ly6G+ PMNs 24hrs
931 after IT *Lm*.
932 (I) Immunofluorescence (right) and Diff-Quick gram staining of sorted intratumoral
933 Ly6G+ PMNs 24hrs after IT *Lm*. For immunofluorescence: DAPI(blue), Lm-RFP (red),
934 Ly6G (green). Scale bar = 20 μm. For Diff-Quick: Scale bar = 50 μm
935 For all plots, mean ± s.e.m. and *P<0.05, **P<0.01, ***P<0.001 by two-way ANOVA (D-
936 E) or student t-test (F, G, H).
937
938 **Figure 3 | PMN conversion into MDSCs permits *Lm* infection and promotes tumor**
939 **growth.**
940 (A-B) Frequency of $CD14^+$ cells amongst $Ly6G^+$ (A) or RFP^+Ly6G^+ cells (B) from MC38
941 tumors 4 and 24 hours after IT PBS or IT *Lm*. Results are pooled from three
942 experiments with n= 2-5 mice/group per experiment.
943 (C) Expression of indicated genes by qPCR analysis from bone marrow (BM), spleen, or
944 tumor of MC38-bearing mice. Results from n= 6 mice from a single experiment.

945 (D) Experimental strategy and representative flow plots for *in vitro* differentiation of
946 conditionally immortalized neutrophil (CIN) progenitors into PMNs (top) or PMN-MDSCs
947 (bottom).
948 (E) PMNs derived from CINs were cultured with conditioned supernatants from 3T3,
949 MC38, or B16F10 cells for 24 hours *in vitro* and the frequency of $CD14^{+}PD\text{-}L1^{+}$ cells
950 was assessed compared to unconditioned media or IL6+GM-CSF treatment
951 (representative of two experiments).
952 (F) Heterogeneous $CD14^{+/-}$ PMNs differentiated from CINs as in (A) were infected with
953 *Lm-RFP in vitro* and Tag-RFP^{+} cells were identified 2, 4, or 8 hours later in all cells
954 (Total PMNs), $CD14^{+}$ cells, or $CD14^{-}$ cells by flow cytometry (representative of three
955 experiments).
956 (G) Representative flow plots of IFNγ production from OT-I CD8 T cells after 24 hour co-
957 culture with MC38 or MC38-OVA tumors in the presence or absence of FACS-purified
958 PMNs from spleens or tumors of IT *Lm*-treated MC38-bearing mice.
959 (H) Quantification of the frequency of $IFN\gamma^{+}$ OT-1 CD8 T cells (G). Cells were plated at
960 a 1:1 ratio of OT-1 T cells to PMNs. Results from 2 independent experiments.
961 (I) Experimental design to deplete PMNs prior to IT PBS or IT *Lm* and measure tumors.
962 (J) Tumor growth measured in mice injected IT with *Lm* (left) or IT PBS (right) and either
963 an isotype control antibody or anti-Ly6G-depleting antibodies prior to tumor inoculation
964 and throughout the experiment (n=5 mice/group from one of two independent
965 experiments).
966 For all plots, *P<0.05, **P<0.01, ***P<0.001 by one-way Anova (B, F) or two-way
967 ANOVA (C, E), mean ± s.e.m for *in vivo* experiments (E) or mean ± s.d. for *in vitro*
968 experiments (B-C, G).
969
970 **Figure 4 | IV+IT *Lm* controls multiple tumor types while clearing intratumoral**
971 **bacteria and PMN-MDSCs from tumors.**
972 (A) Experimental strategy for IV+IT *Lm* dosing regimen.
973 (B-C) IV+IT PBS versus IV+IT *Lm* regimen and growth of MC38 (B, data shown from n=
974 4-5 mice per group from one of three experiments) and B16F10 (C, data shown from n=
975 5-6 mice per group from one of two experiments) tumors.
976 (D) Frequency of $Ly6G^{+}$ PMNs of all $CD45^{+}$ cells one day (left) and 5 days (right) after
977 *Lm* IT in IV+IT *Lm* regimen (data shown from n= 5 mice per group from two pooled
978 experiments).
979 (E) Percent of $Ly6G^{+}$ PMNs that were $CD14^{+}$ 1 day (left) and 5 days (right) after IT *Lm*
980 in IV+IT *Lm* regimen.
981 (F) CFU analysis for *Lm* after IV+IT *Lm* regimen in MC38 tumor-bearing mice. Organs
982 were harvested 4 hours, 12 hours, and on days 1, 3, 5, 10, 15, and 20 after IT *Lm*
983 administration.

984 (G) Experimental design for comparing prophylactic IV Lm (memory IV+IT) to standard
985 IV+IT *Lm* dosing regimen.
986 (H) MC38 tumor growth in the setting of memory IV+IT, memory IV only, and memory
987 IV+SubQ *Lm* (injected on opposing flank) compared to PBS treatment or standard IV+IT
988 *Lm*.
989 (I) Orthotopic KP sarcoma growth with PBS versus a memory IV+IT *Lm* dosing regimen.
990 For all plots, *P<0.05, **P<0.01, ***P<0.001 by student t-test (C, D, E) or two-way
991 ANOVA (B, C, H, I), mean ± s.e.m.
992
993 **Figure 5 | CD8$^+$ T cells are required for tumor control with IV+IT *Lm*.**
994 (A) Experimental strategy for IV+IT *Lm* dosing regimen followed by early or late flow
995 cytometry analysis.
996 (B-C) Frequency of intratumoral CD8$^+$ (B) or CD4$^+$ (C) T cells of CD45$^+$ cells from MC38
997 tumors at early (left) or late (right) timepoints as specified in (A) (results pooled from
998 four experiments with 5 mice/group).
999 (D) Representative flow plots for IFNγ and TNFα intracellular cytokine staining from
1000 intratumoral CD8 T cells 8 days after IT *Lm* or IT PBS administration in each *Lm* dosing
1001 regimen (results pooled from two experiments with 5 mice/group).
1002 (E) Experimental strategy for IV+IT *Lm* dosing regimen plus anti-CD8, anti-CD4, or both
1003 depleting antibodies beginning 10 days after MC38 tumor inoculation.
1004 (F) MC38 tumor growth with T cell depletion.
1005 (G) Frequency of intratumoral Ly6G$^+$ PMNs of CD45$^+$ cells in IV+IT *Lm* treated mice +/-
1006 anti-CD8 depleting antibodies at end of experiment from (F).
1007 (H) MC38 tumor growth in WT versus *Batf3*$^{-/-}$ mice treated with IV+IT *Lm*.
1008 For all plots, *P<0.05, **P<0.01, ***P<0.001 by student t-test (B-C, G), one-way ANOVA
1009 (D), or two-way ANOVA (F, H), mean ± s.e.m.
1010
1011 **Figure 6 | Anti-*Listeria* CD8 immunity mediates tumor control.**
1012 (A) Experimental design to analyze *Lm*-specific CD8 T cells after IV+IT *Lm* (right)
1013 frequency (middle) and total number (left) of *Lm*-specific (SIIN-H2K^b tetramer) CD8 T
1014 cells from MC38 tumors 8 days after IT *Lm-OVA* in IV+IT *Lm-OVA* regimen. OVA was
1015 expressed from *Lm* as a surrogate *Lm* antigen.
1016 (B) Experimental strategy to adoptively transfer *in vitro*-activated OT-I CD8 T cells in
1017 place of prophylactic IV *Lm* and MC38 tumors measured after IT PBS, *Lm*, or *Lm-OVA*
1018 (n= 5-6 mice/group from one of two experiments).
1019 (C) As in (B) but using an orthotopic KP sarcoma model (n= 5-6 mice/group from one of
1020 two independent experiments).
1021 (D) As in (B) but IT delivery compared MC38 tumors grown in WT or β2m$^{-/-}$ mice (left) or
1022 MC38-*B2m*$^{-/-}$ tumors grown in WT or β2m$^{-/-}$ mice (right) (n= 5-6 mice per group).
1023 (E) As in (B) but in *Rag2*$^{-/-}$ mice (n= 5-6 mice/group).

1024 (F) MC38-B2m$^{-/-}$ tumor growth after IV+IT *Lm* or IV+IT PBS plus anti-NK1.1 beginning
1025 10 days after MC38-B2m$^{-/-}$ tumor inoculation (n= 5-6 mice/group).
1026 (G) Experimental strategy to adoptively transfer *in vitro*-activated *Lm*-specific CD8 and
1027 CD4 T cells in place of prophylactic IV *Lm* and MC38 tumors measured after IT PBS or
1028 *Lm* plus anti-CD8 or anti-CD4 beginning 10 days after MC38 tumor inoculation (n= 5-6
1029 mice/group from one of two experiments).
1030 For all plots, *P<0.05, **P<0.01, ***P<0.001 by student t-test (A) or two-way ANOVA (B-
1031 G), mean ± s.e.m.
1032
1033 **Figure 7 | Anti-*Listeria* CD8 immunity enhances antitumor responses.**
1034 (A) Experimental strategy to adoptively transfer *in vitro* expanded SIIN-specific CD8 T
1035 cells from WT, *Prf1*$^{-/-}$, *IFNγ*$^{-/-}$ mice immunized with *Lm-OVA* (see methods).
1036 (B) MC38 tumor growth after adoptive transfer of SIIN-specific CD8 T cells from WT,
1037 IFNγ$^{-/-}$, or *Prf1*$^{-/-}$ mice followed by IT injection of PBS, *Lm*, or *Lm-OVA* at day 11 of tumor
1038 growth (n= 6 mice/group from one of two experiments).
1039 (C) MC38 tumor growth plus anti-TNFα beginning 10 days after MC38-B2m$^{-/-}$ tumor
1040 inoculation (n= 5-6 mice/group from one of two experiments)
1041 (D) Representative images of Cleaved-Caspase 3 (CC3) (green) in MC38 tumors 24
1042 hours post injection with IT PBS, IT *Lm*, or IV+IT *Lm* +/- anti-CD8 i.p. Scale bar =
1043 2000μm. See Fig S7 for additional stains and day 10 images.
1044 (E) Representative images of phospho-Histone 3 (PHH3) (green) in MC38 tumors 24
1045 hours post injection with IT PBS, IT *Lm*, IV+IT *Lm* +/- anti-CD8 i.p. and quantification of
1046 PHH3 staining in MC38 tumors in each group 1 day and 10 days after IT injections.
1047 Scale bar = 2000μm. Inset = high resolution images of boxed section of tissue. See Fig
1048 S7 for additional stains and day 10 images.
1049 (F) Experimental design for the analysis of frequency (left) and total number (right) of
1050 tumor-specific CD8 T cells (MuLV-H2K^{b} tetramer) 8 days after IT *Lm-OVA* in IV+IT *Lm-*
1051 *OVA* regimen compared to IV+IT PBS or IV *Lm-OVA* only.
1052 (G) Frequency of PD-1^{High} (left), Lag3^{+}(center), and PD-1^{High}Lag3^{+} double-positive (right)
1053 tumor-specific (MuLV-H2K^{b} tetramer) CD8 T cells from MC38 tumors 31 days after PBS
1054 or IV+IT *Lm*.
1055 (H) In vitro activated OT-I CD8 T cells were adoptively transferred into WT or *Batf3*$^{-/-}$
1056 mice, MC38 tumors inoculated, and then tumors were injected IT on day 11 with *Lm* or
1057 *Lm*-OVA and tumor growth monitored (n= 5-6 mice per group pooled from two
1058 experiments).
1059 (I) Frequency of tumor-specific (MuLV-H2K^{b} tetramer) CD8 T cells from tumors at end of
1060 experiment in (H).
1061 (J) Representative histogram plots and quantification of 25D1.16 staining (anti-SIIN-
1062 H2K^{b}) on intratumoral cDC1s (MHCII^{+}CD11c^{+}XCR1^{+}) in OVA-expressing *B2m*-deficient
1063 MC38 tumors 24 hours post IT PBS, IT *Lm*, or IV+IT *Lm*.

1064 (K) Adoptive transfer of *Lm*-specific OT-I T cells (as in Figure 6B) was done into T cell
1065 depleter mice (*CD4-Cre; R26*$^{LSL-DTR}$) that were treated with DT beginning 10 days after
1066 MC38 tumor inoculation and tumor growth was monitored (n= 5-6 mice per group
1067 pooled from two experiments).
1068 For all plots, *P<0.05, **P<0.01, ***P<0.001 by student t-test (F-G, I) or two-way
1069 ANOVA (B-C, H, J), mean ± s.e.m.
1070
1071 **Figure S1 | Intravenous injection of *Lm* alone does not slow tumor growth.**
1072 (A) Tumor growth curves for individual mice in 1B.
1073 (B) Tumor growth curves for individual mice in 1C.
1074 (C) Experimental design.
1075 (D-E) C57BL/6J WT mice were injected with $5x10^5$ MC38 (B, data shown from n= 5
1076 mice per group from one of three experiments) or $2x10^5$ B16F10 (C, data shown from
1077 n= 5 mice per group from one of two experiments) tumor cells and then $1x10^6$ *Lm* CFUs
1078 IV 4 days later and tumors measured.
1079 (F) CFU analysis for *Lm* in MC38 tumors from mice injected IV with $1x10^6$ CFU 4 days
1080 after tumor inoculation showed seeding and persistence of *Lm* in tumors as in (B) (n=4-
1081 5 mice per time point).
1082 For all plots, statistical analysis was done by two-way ANOVA, mean ± s.e.m.
1083
1084 **Figure S2 | Population analysis during intratumoral *Lm* infection in MC38 and**
1085 **B16F10 tumors.**
1086 (A) Gating strategy for identifying immune cell subsets from single cell suspension of
1087 MC38 tumor.
1088 (B) Proportion of immune cell types that were $CD45^+RFP^+$ from B16F10 tumors 24
1089 hours after IT *Lm* (n= 4-5 mice/ group).
1090 (C-D) Frequency of intratumoral immune cell populations as percent of all $CD45^+$ cells
1091 24 hours after IT PBS or *Lm* injection in MC38 (C) or B16F10 (D) tumors (n=4-5
1092 mice/group).
1093 (E) Frequency of $Ly6G^+$ PMNs in spleen and B16F10 tumors 24 hours after IT PBS or
1094 IT *Lm* (n=4-5 mice/group).
1095 (F) Frequency of intratumoral $Ly6G^+$ PMNs that were RFP^+ 24 hours after IT *Lm* in
1096 B16F10 tumors.
1097 (G) Validation of anti-Ly6G staining on frozen tumor sections by testing sections from
1098 mice treated with an isotype control antibody or an anti-Gr1 antibody that depletes all
1099 Ly6G+ cells.
1100 For all plots, mean ± s.e.m. and *P<0.05, **P<0.01, ***P<0.001 by student t-test (B, C,
1101 E, F, G, H).
1102
1103 **Figure S3 | PMN-MDSCs are permissive to *Lm* infection.**

1104 (A) Frequency of CD14+ PMNs 24 hours after IT *Lm* in B16F10 tumors. Results from
1105 n= 4-5 mice/group
1106 (B) Frequency of intratumoral CD14+Ly6G$^+$ cells that were RFP$^+$ 24 hours after IT PBS
1107 or IT *Lm*.
1108 (C) Representative flow cytometry plots of the differentiation of primary bone marrow
1109 progenitors into CD14$^+$ PMN-MDSCs *in vitro* by culturing with IL-6 and GM-CSF.
1110 (D) Heterogeneous PMN-MDSCs differentiated from bone marrow progenitors as in (A)
1111 were infected with *Lm-RFP in vitro* and Tag-RFP$^+$ cells were identified 4 or 8 hours later
1112 in all cells (Total PMNs), CD14$^+$ cells, or CD14$^-$ cells by flow cytometry.
1113 (E) Tumor growth curves for individual mice in 3J.
1114 (F) *Lm* CFUs recovered from tumors 20 days after IT *Lm* in mice treated with isotype
1115 control or anti-Ly6G antibodies as shown in Figure 3J.
1116 (G) Proportion of immune cell types that were RFP$^+$ from MC38 tumors treated with an
1117 isotype control (left) or anti-Ly6G antibody (right) 24 hours after IT *Lm*.
1118 (H) Frequency of intratumoral immune cell populations as percent of all CD45$^+$ cells 24
1119 hours after IT *Lm* or IT PBS into MC38 tumors in mice pre-treated with isotype or anti-
1120 Ly6G (PMN-depleting) antibodies as shown in Figure 3I.
1121 For all plots, *P<0.05, **P<0.01, ***P<0.001 by student t-test (A-B, F, H), or one-way
1122 ANOVA (D), mean ± s.d for *in vitro* experiments. Two-way ANOVA (J), mean ± s.e.m for
1123 *in vivo* experiments
1124
1125 **Figure S4 | IV+IT *Lm* is not impacted by PMN depletion and IV+IT regimen leads**
1126 **to *Lm* clearance.**
1127 (A) Tumor growth curves for individual mice in 4B.
1128 (B) Tumor growth curves for individual mice in 4C.
1129 (C) Average (right) and individual tumor growth (left) for MC38 with IV+IV PBS versus
1130 IV+IV *Lm* versus IV+IT *Lm* regimen (data shown from n= 5-6 mice per group from one
1131 of two experiments).
1132 (D) Average (right) and individual tumor growth (left) for MC38 tumor growth with PBS
1133 versus IV+IT *Lm* and with or without anti-Ly6G depleting antibody treatment beginning
1134 two days prior to IT *Lm* administration (n=4-6 mice per group).
1135 (E) Tumor growth curves for individual mice in 4H.
1136 (F) Tumor growth curves for individual mice in 4I.
1137 For all plots, **P<0.05, **P<0.01, ***P<0.001 by two-way ANOVA (C-D), mean ± s.e.m.
1138
1139 **Figure S5 | IV+IT *Lm* dosing regimen reduces intratumoral Treg frequencies but**
1140 **does not impact T cell frequencies in the spleen.**
1141 (A-B) Frequency of CD8$^+$ (C) and CD4$^+$ (D) T cells from spleens at early or late
1142 timepoints. Data pooled from four experiments with 5 mice/group.

1143 (C) Frequency of intratumoral Foxp3$^+$ Tregs of CD4$^+$ cells from MC38 tumors at early
1144 (left) or late (right) timepoints as specified in Figure 5A.
1145 (D) Frequency of Foxp3$^+$ Tregs of CD4$^+$ cells from spleens at early (left) or late (right)
1146 timepoints.
1147 (E) Tumor growth curves for individual mice in 5F.
1148 (F) Average (right) and individual tumor growth (left) for B16F10 with IV+IT *Lm* dosing
1149 regimen plus anti-CD8, anti-CD4, or both depleting antibodies beginning 10 days after
1150 B16F10 tumor inoculation.
1151 (G) Tumor growth curves for individual mice in 5H.
1152 For plots in S5A-S5D, timepoints are the same as what was described in Figure 5A.
1153 For all plots, *P<0.05, **P<0.01, ***P<0.001 by student t-test (A-D) or two-way ANOVA
1154 (F), mean ± s.e.m.
1155
1156 **Figure S6 | *Lm*-specific CD8 T cells are present in tumors independent of Prf1**
1157 **genotype.**
1158 (A) Representative flow plots for SIIN-H2K^b tetramer staining from tumors of mice
1159 treated with IV+IT PBS compared to IV+IT *Lm-OVA* 8 days after IT injections.
1160 (B) Tumor growth curves for individual mice in 6B.
1161 (C) Tumor growth curves for individual mice in 6C.
1162 (D) Tumor growth curves for individual mice in 6D.
1163 (E) Frequency of intratumoral OT-I CD8 T cells in mice 20 days after IT *Lm*
1164 administration from Figure 6D.
1165 (F) CFU analysis for *Lm* in tumors from Figure 6D.
1166 (G) Tumor growth curves for individual mice in 6E.
1167 (H) Tumor growth curves for individual mice in 6F.
1168 (I) Tumor growth curves for individual mice in 6G.
1169 For all plots, *P<0.05, **P<0.01, ***P<0.001 by student t-test (E-F), mean ± s.e.m.
1170
1171 **Figure S7 | *Antitumor T cell immunity enhancement is dependent on Listeria-***
1172 ***specific direct killing and cytokine secretion*.**
1173 (A-B) Tumor growth curves for individual mice in 7B.
1174 (C) Frequency of intratumoral SIIN-specific CD8 T cells in mice 20 days after IT *Lm*
1175 administration from experiments depicted in Figures 6J-K (pooled from two independent
1176 experiments)
1177 (D) Tumor growth curves for individual mice in 7C.
1178 (E) Images of MC38 tumors 24hrs post injection with IT PBS, IT *Lm*, or given IV+IT
1179 dosing regimen +/- anti-CD8 i.p: phospho-Histone 3 (PHH3) or cleaved-caspase 3
1180 (CC3) (green), WGA (red) and DAPI (blue). Scale bar = 2000μm.

1181 (F) Images of MC38 tumors 10 days post injection with IT PBS, IT *Lm*, or given IV+IT
1182 dosing regimen +/- anti-CD8 i.p: phospho-Histone 3 (PHH3) or cleaved-caspase 3
1183 (CC3) (green), WGA (red) and DAPI (blue). Scale bar = 2000µm.
1184 (G) Representative flow plots for MuLV-H2K^b tetramer staining in lymph nodes from
1185 naive mice compared to MC38 tumor-bearing mice 19 days post tumor inoculation.
1186 (H) Representative flow plots for PD-1+Lag3+ MuLV-H2K^b CD8 T cells for 7G.
1187 (I) Tumor growth curves for individual mice in 7H.
1188 (J) Depletion of T cells in T cell depleter mice (CD4^{Cre}; R26$^{LSL-DTR}$) in non-tumor bearing
1189 mice. Mice were injected twice with 1µg DT i.p. every two days and inguinal lymph
1190 nodes and spleen collected for flow analysis.
1191 (K) Tumor growth curves for individual mice in 7K.
1192 (L) Frequency of intratumoral tumor-specific (MuLV-H2K^b tetramer) CD8 T cells (right)
1193 and OT-I CD8 T (left) cells in mice 20 days after IT *Lm* administration from Figure 7J.
1194 For all plots, *P<0.05, **P<0.01, ***P<0.001 by student t-test (C,M) or two-way ANOVA
1195 (H), mean ± s.e.m.
1196
1197 **References**

1198 1. McCarthy, E. F. The Toxins of William B. Coley and the Treatment of Bone and
1199 Soft-Tissue Sarcomas. *Iowa Orthop. J.* **26**, 154 (2006).
1200 2. Hc, N., Ga, F. & Fh, B. A review of the influence of bacterial infection and of
1201 bacterial products (Coley's toxins) on malignant tumors in man; a critical analysis of
1202 30 inoperable cases treated by Coley's mixed toxins, in which diagnosis was
1203 confirmed by microscopic examination selected for special study. *Acta Med. Scand.*
1204 *Suppl.* **276**, (1953).
1205 3. Hoption Cann, S. A., van Netten, J. P. & van Netten, C. Dr William Coley and
1206 tumour regression: a place in history or in the future. *Postgrad. Med. J.* **79**, 672
1207 (2003).
1208 4. Jiang, S. & Redelman-Sidi, G. BCG in Bladder Cancer Immunotherapy. *Cancers*
1209 **14**, 3073 (2022).
1210 5. Yu, Y. A. *et al.* Visualization of tumors and metastases in live animals with bacteria

1211 and vaccinia virus encoding light-emitting proteins. *Nat. Biotechnol.* **22**, 313–320
1212 (2004).
1213 6. Kang, S.-R. *et al.* Imaging of tumor colonization by Escherichia coli using 18F-FDS
1214 PET. *Theranostics* **10**, 4958 (2020).
1215 7. Fu, A. *et al.* Tumor-resident intracellular microbiota promotes metastatic
1216 colonization in breast cancer. *Cell* **185**, (2022).
1217 8. Riquelme, E. *et al.* Tumor Microbiome Diversity and Composition Influence
1218 Pancreatic Cancer Outcomes. *Cell* **178**, (2019).
1219 9. Poore, G. D. *et al.* Microbiome analyses of blood and tissues suggest cancer
1220 diagnostic approach. *Nature* **579**, (2020).
1221 10. Pushalkar, S. *et al.* The Pancreatic Cancer Microbiome Promotes Oncogenesis by
1222 Induction of Innate and Adaptive Immune Suppression. *Cancer Discov.* **8**, (2018).
1223 11. Jin, C. *et al.* Commensal Microbiota Promote Lung Cancer Development via γδ T
1224 Cells. *Cell* **176**, (2019).
1225 12. Pawelek, J. M., Low, K. B. & Bermudes, D. Tumor-targeted Salmonella as a novel
1226 anticancer vector. *Cancer Res.* **57**, (1997).
1227 13. Dang, L. H., Bettegowda, C., Huso, D. L., Kinzler, K. W. & Vogelstein, B.
1228 Combination bacteriolytic therapy for the treatment of experimental tumors. *Proc.*
1229 *Natl. Acad. Sci. U. S. A.* **98**, (2001).
1230 14. Honda, K. & Littman, D. R. The microbiota in adaptive immune homeostasis and
1231 disease. *Nature* **535**, 75–84 (2016).
1232 15. Battaglia, T. W. *et al.* A pan-cancer analysis of the microbiome in metastatic
1233 cancer. *Cell* **187**, 2324–2335.e19 (2024).

1234 16. Bullman, S. The intratumoral microbiota: From microniches to single cells. *Cell* **186**,
1235 1532–1534 (2023).
1236 17. Zhou, M. *et al.* Bacteria-based immunotherapy for cancer: a systematic review of
1237 preclinical studies. *Front. Immunol.* **14**, (2023).
1238 18. Riglar, D. T. & Silver, P. A. Engineering bacteria for diagnostic and therapeutic
1239 applications. *Nat. Rev. Microbiol.* **16**, 214–225 (2018).
1240 19. Chowdhury, S. *et al.* Programmable bacteria induce durable tumor regression and
1241 systemic antitumor immunity. *Nat. Med.* **25**, (2019).
1242 20. Din, M. O. *et al.* Synchronized cycles of bacterial lysis for in vivo delivery. *Nature*
1243 **536**, (2016).
1244 21. Redenti, A. *et al.* Probiotic neoantigen delivery vectors for precision cancer
1245 immunotherapy. *Nature* **635**, 453–461 (2024).
1246 22. Deng, W. *et al.* Recombinant *Listeria* promotes tumor rejection by $CD8^+$ T cell-
1247 dependent remodeling of the tumor microenvironment. *Proc. Natl. Acad. Sci. U. S.*
1248 *A.* **115**, 8179–8184 (2018).
1249 23. Kim, S. H. *et al.* Mage-b vaccine delivered by recombinant Listeria monocytogenes
1250 is highly effective against breast cancer metastases. *Br. J. Cancer* **99**, 741 (2008).
1251 24. Listeria as a vaccine vector. *Microbes Infect.* **9**, 1226–1235 (2007).
1252 25. Ding, Y. D. *et al.* Listeria monocytogenes: a promising vector for tumor
1253 immunotherapy. *Front. Immunol.* **14**, (2023).
1254 26. Pan, Z.-K., Ikonomidis, G., Lazenby, A., Pardoll, D. & Paterson, Y. A recombinant
1255 Listeria monocytogenes vaccine expressing a model tumour antigen protects mice
1256 against lethal tumour cell challenge and causes regression of established tumours.

1257 *Nat. Med.* **1**, 471–477 (1995).
1258 27. Nguyen, D. H., Chong, A., Hong, Y. & Min, J. J. Bioengineering of bacteria for
1259 cancer immunotherapy. *Nat. Commun.* **14**, (2023).
1260 28. Hassan, R. *et al.* Clinical Response of Live-Attenuated, Listeria monocytogenes
1261 Expressing Mesothelin (CRS-207) with Chemotherapy in Patients with Malignant
1262 Pleural Mesothelioma. *Clin. Cancer Res.* **25**, 5787–5798 (2019).
1263 29. Le, D. T. *et al.* Safety and survival with GVAX pancreas prime and Listeria
1264 Monocytogenes-expressing mesothelin (CRS-207) boost vaccines for metastatic
1265 pancreatic cancer. *J. Clin. Oncol.* **33**, (2015).
1266 30. Huh, W. K. *et al.* Phase II study of axalimogene filolisbac (ADXS-HPV) for platinum-
1267 refractory cervical carcinoma: An NRG oncology/gynecologic oncology group study.
1268 *Gynecol. Oncol.* **158**, (2020).
1269 31. Basu, P. *et al.* A Randomized Phase 2 Study of ADXS11-001 Listeria
1270 monocytogenes-Listeriolysin O Immunotherapy With or Without Cisplatin in
1271 Treatment of Advanced Cervical Cancer. *Int. J. Gynecol. Cancer* **28**, (2018).
1272 32. Drake, C. G. *et al.* Safety and preliminary immunogenicity of JNJ-64041809, a live-
1273 attenuated, double-deleted Listeria monocytogenes-based immunotherapy, in
1274 metastatic castration-resistant prostate cancer. *Prostate Cancer Prostatic Dis.* **25**,
1275 (2022).
1276 33. Stein, M. N. *et al.* ADXS31142 Immunotherapy ± Pembrolizumab Treatment for
1277 Metastatic Castration-Resistant Prostate Cancer: Open-Label Phase I/II
1278 KEYNOTE-046 Study. *Oncologist* **27**, (2022).
1279 34. Moreno Ayala, M. A., Li, Z. & DuPage, M. Treg programming and therapeutic

1280 reprogramming in cancer. *Immunology* **157**, 198–209 (2019).
1281 35. Veglia, F., Sanseviero, E. & Gabrilovich, D. I. Myeloid-derived suppressor cells in
1282 the era of increasing myeloid cell diversity. *Nat. Rev. Immunol.* **21**, 485–498 (2021).
1283 36. Li, K. *et al.* Myeloid-derived suppressor cells as immunosuppressive regulators and
1284 therapeutic targets in cancer. *Signal Transduction and Targeted Therapy* **6**, (2021).
1285 37. Binnewies, M. *et al.* Understanding the tumor immune microenvironment (TIME) for
1286 effective therapy. *Nat. Med.* **24**, (2018).
1287 38. Perry, C. J. *et al.* Myeloid-targeted immunotherapies act in synergy to induce
1288 inflammation and antitumor immunity. *J. Exp. Med.* **215**, 877–893 (2018).
1289 39. Ostrand-Rosenberg, S. & Fenselau, C. Myeloid-derived suppressor cells: Immune
1290 suppressive cells that impair antitumor immunity and are sculpted by their
1291 environment. *J. Immunol.* **200**, 422 (2018).
1292 40. Gabrilovich, D. I. Myeloid-derived suppressor cells. *Cancer immunology research* **5**,
1293 3 (2017).
1294 41. Long, A. H. *et al.* Reduction of MDSCs with all-trans retinoic acid improves CAR
1295 therapy efficacy for sarcomas. *Cancer immunology research* **4**, 869 (2016).
1296 42. Zhu, J. *et al.* Resistance to cancer immunotherapy mediated by apoptosis of tumor-
1297 infiltrating lymphocytes. *Nat. Commun.* **8**, (2017).
1298 43. Cao, L. L. & Kagan, J. C. Targeting innate immune pathways for cancer
1299 immunotherapy. *Immunity* **56**, (2023).
1300 44. Uher, O. *et al.* Coley's immunotherapy revived: Innate immunity as a link in priming
1301 cancer cells for an attack by adaptive immunity. *Semin. Oncol.* **46**, (2019).
1302 45. Marabelle, A., Kohrt, H., Caux, C. & Levy, R. Intratumoral immunization: a new

1303 paradigm for cancer therapy. *Clin. Cancer Res.* **20**, (2014).
1304 46. Frank, M. J. *et al.* In Situ Vaccination with a TLR9 Agonist and Local Low-Dose
1305 Radiation Induces Systemic Responses in Untreated Indolent Lymphoma. *Cancer*
1306 *Discov.* **8**, (2018).
1307 47. Nicolai, C. J. *et al.* NK cells mediate clearance of CD8+ T cell-resistant tumors in
1308 response to STING agonists. *Science immunology* **5**, (2020).
1309 48. Xu, G. *et al.* Listeria-based hepatocellular carcinoma vaccine facilitates anti-PD-1
1310 therapy by regulating macrophage polarization. *Oncogene* **39**, 1429–1444 (2019).
1311 49. Wang, Y. *et al.* Adjuvant effect of the novel TLR1/TLR2 agonist Diprovocim
1312 synergizes with anti-PD-L1 to eliminate melanoma in mice. *Proc. Natl. Acad. Sci. U.*
1313 *S. A.* **115**, E8698–E8706 (2018).
1314 50. Corrales, L. *et al.* Direct Activation of STING in the Tumor Microenvironment Leads
1315 to Potent and Systemic Tumor Regression and Immunity. *Cell Rep.* **11**, (2015).
1316 51. Oladejo, M., Paterson, Y. & Wood, L. M. Clinical Experience and Recent Advances
1317 in the Development of Listeria-Based Tumor Immunotherapies. *Front. Immunol.* **12**,
1318 642316 (2021).
1319 52. Brockstedt, D. G. *et al.* Listeria-based cancer vaccines that segregate
1320 immunogenicity from toxicity. *Proc. Natl. Acad. Sci. U. S. A.* **101**, 13832–13837
1321 (2004).
1322 53. Miyabayashi, K. *et al.* Intraductal Transplantation Models of Human Pancreatic
1323 Ductal Adenocarcinoma Reveal Progressive Transition of Molecular Subtypes.
1324 *Cancer Discov.* **10**, 1566–1589 (2020).
1325 54. Waite, J. C. *et al.* Dynamic imaging of the effector immune response to listeria

1326 infection in vivo. *PLoS Pathog.* **7**, (2011).
1327 55. Moors, M. A., Levitt, B., Youngman, P. & Portnoy, D. A. Expression of listeriolysin
1328 O and ActA by intracellular and extracellular Listeria monocytogenes. *Infect.*
1329 *Immun.* **67**, (1999).
1330 56. Czuprynski, C. J., Henson, P. M. & Campbell, P. A. Killing of Listeria
1331 monocytogenes by Inflammatory Neutrophils and Mononuclear Phagocytes From
1332 Immune and Nonimmune Mice. *J. Leukoc. Biol.* **35**, 193–208 (1984).
1333 57. Witter, A. R., Okunnu, B. M. & Berg, R. E. The Essential Role of Neutrophils during
1334 Infection with the Intracellular Bacterial Pathogen Listeria monocytogenes. *J.*
1335 *Immunol.* **197**, 1557–1565 (2016).
1336 58. Okunnu, B. M. & Berg, R. E. Neutrophils Are More Effective than Monocytes at
1337 Phagosomal Containment and Killing of Listeria monocytogenes. *ImmunoHorizons*
1338 **3**, (2019).
1339 59. Shaul, M. E. & Fridlender, Z. G. Neutrophils as active regulators of the immune
1340 system in the tumor microenvironment. *J. Leukoc. Biol.* **102**, 343–349 (2017).
1341 60. Powell, D. R. & Huttenlocher, A. Neutrophils in the Tumor Microenvironment.
1342 *Trends Immunol.* **37**, 41–52 (2016).
1343 61. Roberts, A. W. *et al.* Cas9+ conditionally-immortalized macrophages as a tool for
1344 bacterial pathogenesis and beyond. *Elife* **8**, (2019).
1345 62. Veglia, F. *et al.* Analysis of classical neutrophils and polymorphonuclear myeloid-
1346 derived suppressor cells in cancer patients and tumor-bearing mice. *J Exp Med*
1347 **218**, (2021).
1348 63. Eckert, I., Ribechini, E. & Lutz, M. B. In Vitro Generation of Murine Myeloid-Derived

1349 Suppressor Cells, Analysis of Markers, Developmental Commitment, and Function.
1350 *Myeloid-Derived Suppressor Cells* 99–114 (2021).
1351 64. Wu, Y., Yi, M., Niu, M., Mei, Q. & Wu, K. Myeloid-derived suppressor cells: an
1352 emerging target for anticancer immunotherapy. *Mol. Cancer* **21**, 1–19 (2022).
1353 65. Chávez-Arroyo, A. & Portnoy, D. A. Why is Listeria monocytogenes such a potent
1354 inducer of CD8+ T-cells? *Cell. Microbiol.* **22**, e13175 (2020).
1355 66. Genitourinary cancer neoadjuvant therapies: current and future approaches.
1356 *Trends Cancer Res.* **9**, 1041–1057 (2023).
1357 67. Kirsch, D. G. *et al.* A spatially and temporally restricted mouse model of soft tissue
1358 sarcoma. *Nat. Med.* **13**, (2007).
1359 68. Waldman, A. D., Fritz, J. M. & Lenardo, M. J. A guide to cancer immunotherapy:
1360 from T cell basic science to clinical practice. *Nat. Rev. Immunol.* **20**, 651–668
1361 (2020).
1362 69. Giles, J. R., Globig, A. M., Kaech, S. M. & Wherry, E. J. CD8+ T cells in the cancer-
1363 immunity cycle. *Immunity* **56**, (2023).
1364 70. Wang, D. *et al.* Targeting EZH2 Reprograms Intratumoral Regulatory T Cells to
1365 Enhance Cancer Immunity. *Cell Rep.* **23**, (2018).
1366 71. Moreno Ayala, M. A. *et al.* CXCR3 expression in regulatory T cells drives
1367 interactions with type I dendritic cells in tumors to restrict CD8+ T cell antitumor
1368 immunity. *Immunity* **56**, 1613–1630.e5 (2023).
1369 72. Hos, B. J. *et al.* Identification of a neo-epitope dominating endogenous CD8 T cell
1370 responses to MC-38 colorectal cancer. *Oncoimmunology* **9**, 1673125 (2019).
1371 73. Liu, D. *et al.* IL-10-Dependent Crosstalk between Murine Marginal Zone B Cells,

1372 Macrophages, and CD8α+ Dendritic Cells Promotes Listeria monocytogenes
1373 Infection. *Immunity* **51**, 64–76.e7 (2019).
1374 74. Edelson, B. T. *et al.* CD8α(+) dendritic cells are an obligate cellular entry point for
1375 productive infection by Listeria monocytogenes. *Immunity* **35**, (2011).
1376 75. DuPage, M., Mazumdar, C., Schmidt, L. M., Cheung, A. F. & Jacks, T. Expression
1377 of tumour-specific antigens underlies cancer immunoediting. *Nature* **482**, (2012).
1378 76. Selvanesan, B. C. *et al.* Listeria delivers tetanus toxoid protein to pancreatic tumors
1379 and induces cancer cell death in mice. *Sci. Transl. Med.* **14**, eabc1600 (2022).
1380 77. Martínez-Sabadell, A., Arenas, E. J. & Arribas, J. IFNγ Signaling in Natural and
1381 Therapy-Induced Antitumor Responses. *Clin Cancer Res* **28**, 1243–1249 (2022).
1382 78. Memarnejadian, A. *et al.* PD-1 Blockade Promotes Epitope Spreading in Anticancer
1383 CD8 T Cell Responses by Preventing Fratricidal Death of Subdominant Clones To
1384 Relieve Immunodomination. *J Immunol* **199**, 3348–3359 (2017).
1385 79. Conde, E. *et al.* Epitope spreading driven by the joint action of CART cells and
1386 pharmacological STING stimulation counteracts tumor escape via antigen-loss
1387 variants. *J Immunother Cancer* **9**, e003351 (2021).
1388 80. Roberts, E. W. *et al.* Critical Role for CD103(+)/CD141(+) Dendritic Cells Bearing
1389 CCR7 for Tumor Antigen Trafficking and Priming of T Cell Immunity in Melanoma.
1390 *Cancer Cell* **30**, 324–336 (2016).
1391 81. Salmon, H. *et al.* Expansion and Activation of CD103(+) Dendritic Cell Progenitors
1392 at the Tumor Site Enhances Tumor Responses to Therapeutic PD-L1 and BRAF
1393 Inhibition. *Immunity* **44**, 924–938 (2016).
1394 82. Imperato, J. N. *et al.* Mucosal CD8 T Cell Responses Are Shaped by Batf3-DC

1395 After Foodborne Listeria monocytogenes Infection. *Frontiers in immunology* **11**,
1396 (2020).
1397 83. Buch, T. *et al.* A Cre-inducible diphtheria toxin receptor mediates cell lineage
1398 ablation after toxin administration. *Nature methods* **2**, (2005).
1399 84. Leschner, S. *et al.* Tumor invasion of Salmonella enterica serovar Typhimurium is
1400 accompanied by strong hemorrhage promoted by TNF-alpha. *PLoS One* **4**, e6692
1401 (2009).
1402 85. Jiang, S.-N. *et al.* Inhibition of tumor growth and metastasis by a combination of
1403 Escherichia coli-mediated cytolytic therapy and radiotherapy. *Mol. Ther.* **18**, 635–
1404 642 (2010).
1405 86. Agrawal, N. *et al.* Bacteriolytic therapy can generate a potent immune response
1406 against experimental tumors. *Proc. Natl. Acad. Sci. U. S. A.* **101**, (2004).
1407 87. St. Jean, A. T., Swofford, C. A., Panteli, J. T., Brentzel, Z. J. & Forbes, N. S.
1408 Bacterial Delivery of Staphylococcus aureus α-Hemolysin Causes Regression and
1409 Necrosis in Murine Tumors. *Mol. Ther.* **22**, 1266–1274 (2014).
1410 88. Canale, F. P. *et al.* Metabolic modulation of tumours with engineered bacteria for
1411 immunotherapy. *Nature* **598**, (2021).
1412 89. Ahmed, S. G. *et al.* Intratumoral injection of schwannoma with attenuated induces
1413 antitumor immunity and controls tumor growth. *Proc. Natl. Acad. Sci. U. S. A.* **119**,
1414 e2202719119 (2022).
1415 90. Weibel, S., Stritzker, J., Eck, M., Goebel, W. & Szalay, A. A. Colonization of
1416 experimental murine breast tumours by Escherichia coli K-12 significantly alters the
1417 tumour microenvironment. *Cell. Microbiol.* **10**, (2008).

1418 91. Quispe-Tintaya, W. *et al.* Nontoxic radioactive Listeria(at) is a highly effective
1419 therapy against metastatic pancreatic cancer. *Proc. Natl. Acad. Sci. U. S. A.* **110**,
1420 8668–8673 (2013).
1421 92. Jia, L.-J. *et al.* Enhanced therapeutic effect by combination of tumor-targeting
1422 salmonella and endostatin in murine melanoma model. *Cancer Biol. Ther.* (2005)
1423 doi:10.4161/cbt.4.8.1891.
1424 93. Westphal, K., Leschner, S., Jablonska, J., Loessner, H. & Weiss, S. Containment of
1425 tumor-colonizing bacteria by host neutrophils. *Cancer Res.* **68**, (2008).
1426 94. Kim, M. *et al.* Critical Role for the Microbiota in CX3CR1+ Intestinal Mononuclear
1427 Phagocyte Regulation of Intestinal T Cell Responses. *Immunity* **49**, (2018).
1428 95. Delivery of a viral antigen to the class I processing and presentation pathway by
1429 Listeria monocytogenes. *J. Exp. Med.* **180**, 2209 (1994).
1430 96. Raskov, H., Orhan, A., Christensen, J. P. & Gögenur, I. Cytotoxic CD8+ T cells in
1431 cancer and cancer immunotherapy. *Br. J. Cancer* **124**, 359–367 (2021).
1432 97. Biot, C. *et al.* Preexisting BCG-specific T cells improve intravesical immunotherapy
1433 for bladder cancer. *Sci. Transl. Med.* **4**, (2012).
1434 98. Aqbi, H. F., Wallace, M., Sappal, S., Payne, K. K. & Manjili, M. H. IFN-γ
1435 orchestrates tumor elimination, tumor dormancy, tumor escape, and progression. *J*
1436 *Leukoc Biol* (2018) doi:10.1002/JLB.5MIR0917-351R.
1437 99. Li, F. *et al.* Programmable bacteria synergize with PD-1 blockade to overcome
1438 cancer cell-intrinsic immune resistance mechanisms. *Sci Immunol* **9**, eadn9879
1439 (2024).
1440 100. van Loo, G. & Bertrand, M. J. M. Death by TNF: a road to inflammation. *Nature*

1441 *Reviews Immunology* **23**, 289–303 (2022).
1442 101. Xin, G. *et al.* Pathogen-Boosted Adoptive Cell Transfer Therapy Induces
1443 Endogenous Antitumor Immunity through Antigen Spreading. *Cancer Immunol Res*
1444 **8**, 7–18 (2020).
1445 102. Chen, X. *et al.* An oncolytic virus delivering tumor-irrelevant bystander T cell
1446 epitopes induces anti-tumor immunity and potentiates cancer immunotherapy.
1447 *Nature Cancer* **5**, 1063–1081 (2024).
1448 103. Wang, M. *et al.* Killing tumor-associated bacteria with a liposomal antibiotic
1449 generates neoantigens that induce anti-tumor immune responses. *Nat Biotechnol*
1450 **42**, 1263–1274 (2024).
1451 104. Liu, Q., Sun, Z. & Chen, L. Memory T cells: strategies for optimizing tumor
1452 immunotherapy. *Protein Cell* **11**, 549–564 (2020).
1453 105. Sockolosky, J. T. *et al.* Selective targeting of engineered T cells using orthogonal
1454 IL-2 cytokine-receptor complexes. *Science* **359**, 1037–1042 (2018).
1455 106. Bahjat, K. S. *et al.* Cytosolic entry controls CD8+-T-cell potency during bacterial
1456 infection. *Infect. Immun.* **74**, 6387–6397 (2006).
1457 107. Roy, I. *et al.* Pancreatic Cancer Cell Migration and Metastasis Is Regulated by
1458 Chemokine-Biased Agonism and Bioenergetic Signaling. *Cancer Res* **75**, 3529–
1459 3542 (2015).

1460

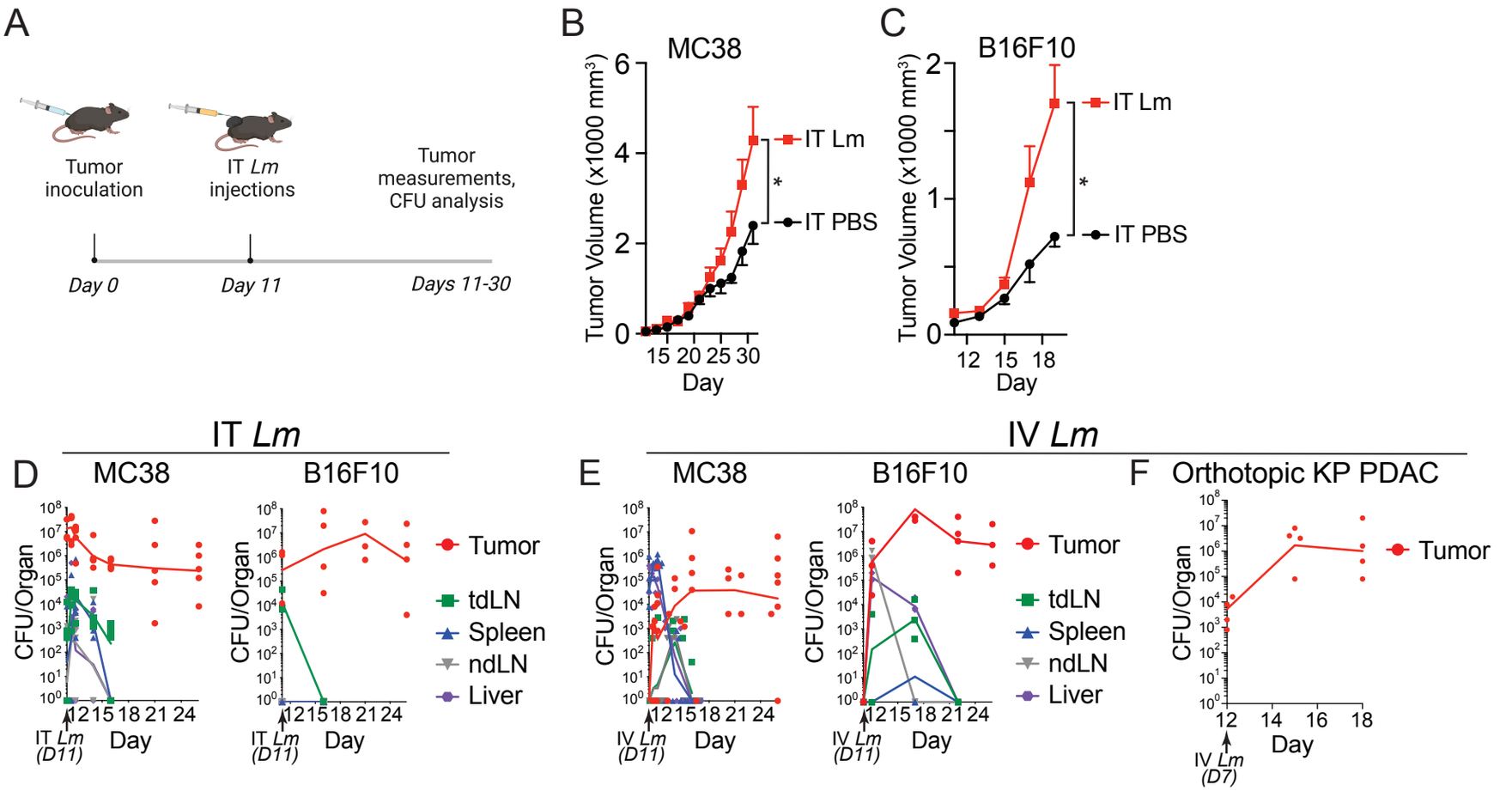

Garcia Castillo, J., Campbell, T., & Fernandez, S. et al. Figure 1.

Figure 1 | Intratumoral injection of *Lm* leads to increased tumor growth and persistent colonization of *Lm* within tumors.

(A) Experimental design.

(B-C) C57BL/6J WT mice were injected with $5x10^5$ MC38 (B, data shown from n= 4-5 mice per group from one of three experiments) or $2x10^5$ B16F10 (C, data shown from n=4-5 mice per group from one of two experiments) tumor cells and then $5x10^7$ *Lm* CFUs IT 11 days later and tumors measured.

(D-E) CFU analysis for *Lm* from indicated tissues after injection IT (D, $5x10^7$ CFU, n=4-8 mice pooled from two experiments) or IV (E, $1x10^6$ CFU, n=4-5 mice pooled from two experiments) of *Lm* 11 days after MC38 or B16F10 tumor inoculation. tdLN = tumor-draining lymph node, ndLN = non-tumor-draining LN.

(F) CFU analysis for *Lm* at indicated time points from PDAC pancreatic tissue after orthotopic transplantation of FC1245[107](n=4 mice). 10^6 CFU of Lm injected on day 7.

For all plots, *P<0.05, **P<0.01 by two-way ANOVA, mean ± s.e.m.

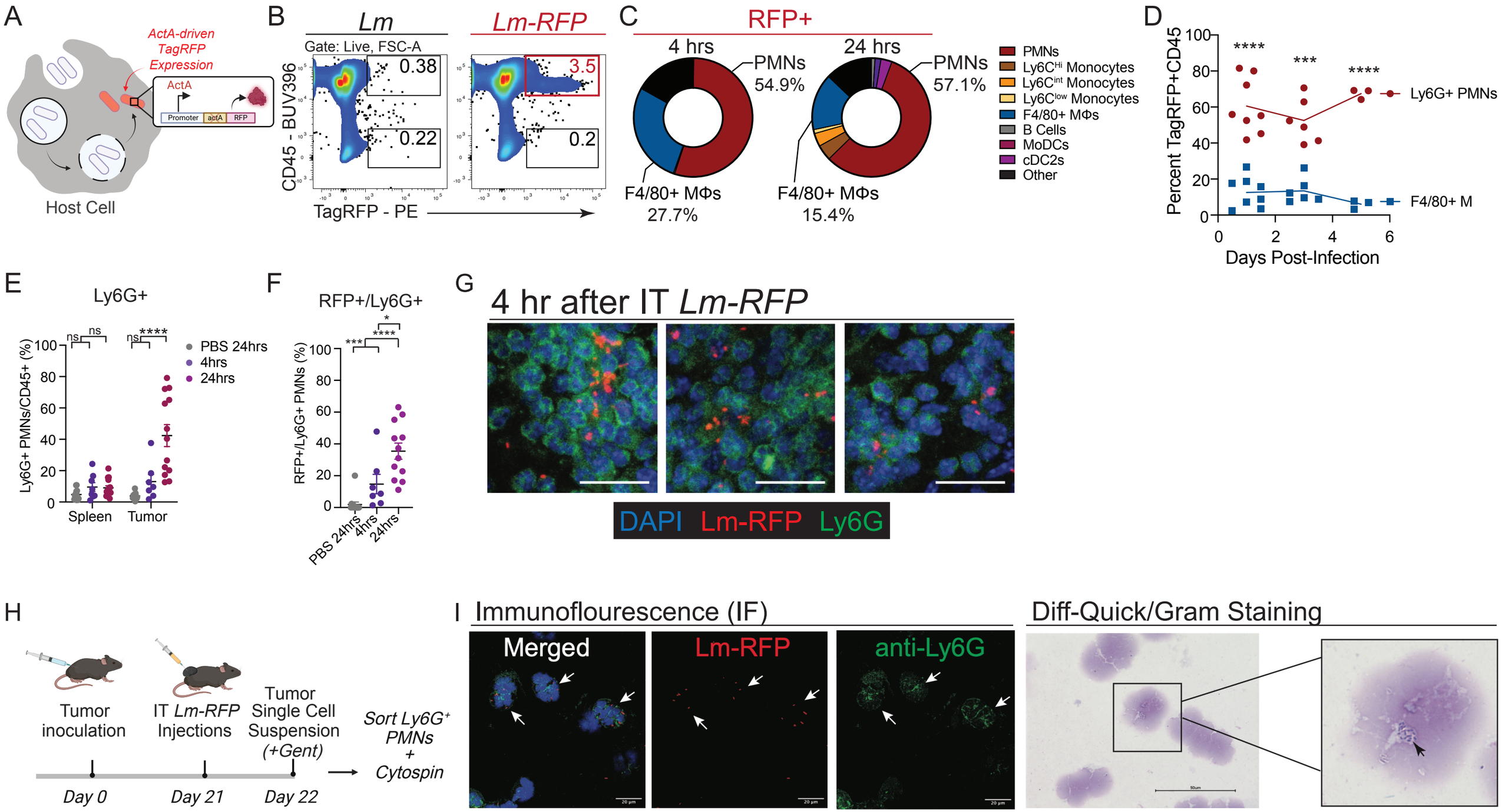

Garcia Castillo, J., Campbell, T., & Fernandez, S. et al. Figure 2

Figure 2 | *Lm* localizes in intratumoral PMNs.

(A) Schematic of Tag-RFP expression from *Lm-RFP*.

(B) Representative flow plots from single cell suspensions of MC38 tumors 4 hours post IT *Lm* (left) or IT *Lm-RFP* (right) showing CD45 staining versus Tag-RFP fluorescence.

(C) Distribution of RFP^+ immune cell types from MC38 tumors at 4 (left) or 24 (right) hours after IT *Lm* (representative data from three experiments with n= 3-6 mice/group).

(D) Analysis of the fraction of PMNs and TAMs that were RFP^+ at 1, 3, and 5 days after IT *Lm-RFP* in MC38 tumors (representative data from two experiments with n= 3-6 mice/group).

(E) Frequency of $Ly6G^+$ PMNs in spleen or tumors from MC38-bearing mice at 4 and 24 hours after IT PBS or IT *Lm*.

(F) Frequency of intratumoral $Ly6G^+$ cells that were RFP^+ at 4 and 24 hours after IT PBS or IT *Lm*. Results in E-F are pooled from three experiments with n= 2-5 mice/group per experiment.

(G) Images of MC38 tumors 4hrs after IT *Lm*: DAPI (blue), *Lm-RFP* (red), Ly6G (green). Scale bar = 20 μm.

(H) Schematic for cytospin imaging analysis of sorted intratumoral Ly6G+ PMNs 24hrs after IT *Lm*.

(I) Immunofluorescence (right) and Diff-Quick gram staining of sorted intratumoral Ly6G+ PMNs 24hrs after IT *Lm*. For immunofluorescence: DAPI(blue), Lm-RFP (red), Ly6G (green). Scale bar = 20 μm. For Diff-Quick: Scale bar = 50 μm

For all plots, mean ± s.e.m. and *P<0.05, **P<0.01, ***P<0.001 by two-way ANOVA (D-E) or student t-test (F, G, H).

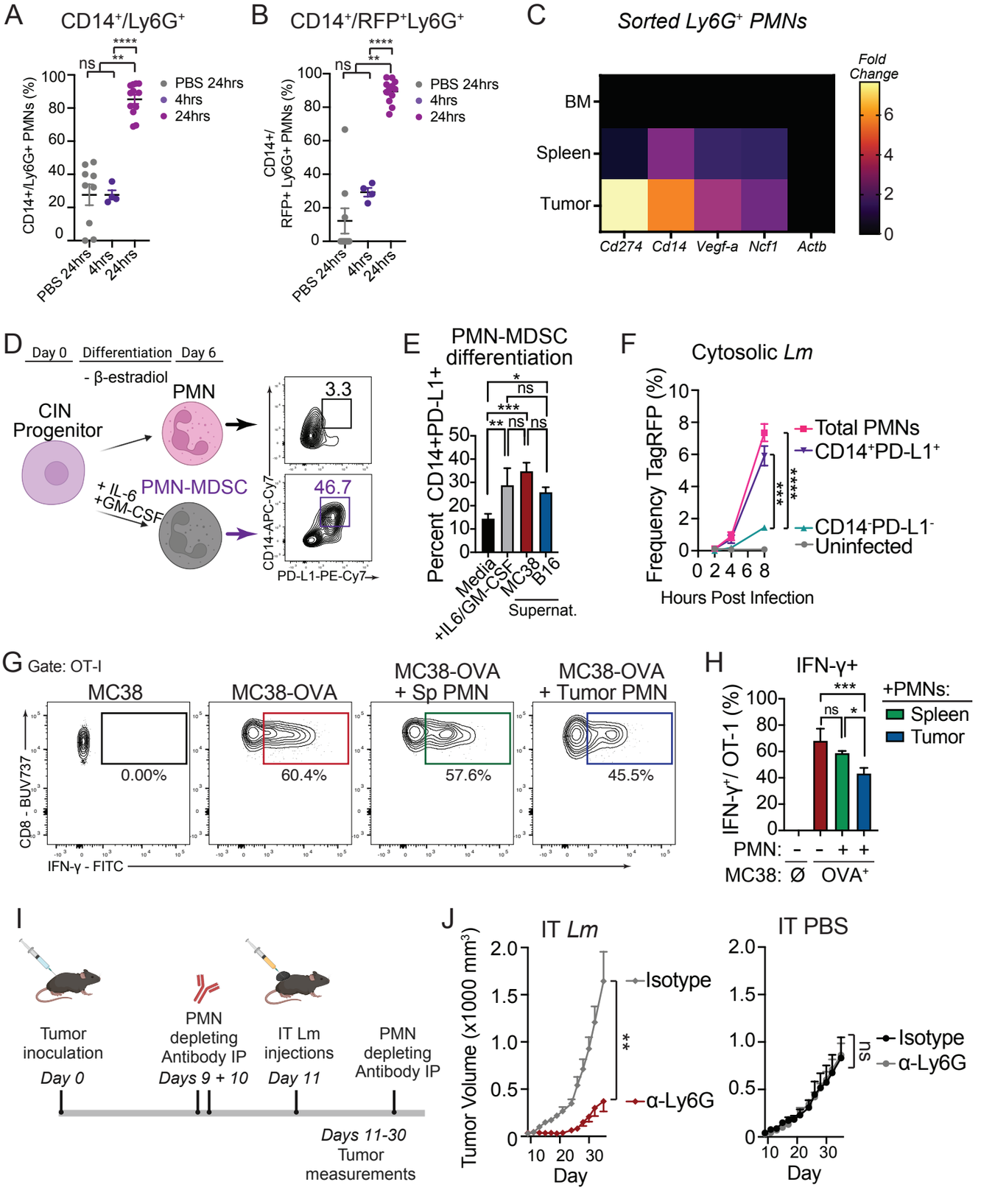

Garcia Castillo, J., Campbell, T., & Fernandez, S. et al. Figure 3.

Figure 3 | PMN conversion into MDSCs permits *Lm* infection and promotes tumor growth.

(A-B) Frequency of $CD14^+$ cells amongst $Ly6G^+$ (A) or RFP^+Ly6G^+ cells (B) from MC38 tumors 4 and 24 hours after IT PBS or IT *Lm*. Results are pooled from three experiments with n= 2-5 mice/group per experiment.

(C) Expression of indicated genes by qPCR analysis from bone marrow (BM), spleen, or tumor of MC38-bearing mice. Results from n= 6 mice from a single experiment.

(D) Experimental strategy and representative flow plots for *in vitro* differentiation of conditionally immortalized neutrophil (CIN) progenitors into PMNs (top) or PMN-MDSCs (bottom).

(E) PMNs derived from CINs were cultured with conditioned supernatants from 3T3, MC38, or B16F10 cells for 24 hours *in vitro* and the frequency of $CD14^+PD\text{-}L1^+$ cells was assessed compared to unconditioned media or IL6+GM-CSF treatment (representative of two experiments).

(F) Heterogeneous $CD14^{+/-}$ PMNs differentiated from CINs as in (A) were infected with *Lm-RFP in vitro* and Tag-RFP^+ cells were identified 2, 4, or 8 hours later in all cells (Total PMNs), $CD14^+$ cells, or $CD14^-$ cells by flow cytometry (representative of three experiments).

(G) Representative flow plots of IFNγ production from OT-I CD8 T cells after 24 hour co-culture with MC38 or MC38-OVA tumors in the presence or absence of FACS-purified PMNs from spleens or tumors of IT *Lm*-treated MC38-bearing mice.

(H) Quantification of the frequency of $IFN\gamma^+$ OT-1 CD8 T cells (G). Cells were plated at a 1:1 ratio of OT-1 T cells to PMNs. Results from 2 independent experiments.

(I) Experimental design to deplete PMNs prior to IT PBS or IT *Lm* and measure tumors.

(J) Tumor growth measured in mice injected IT with *Lm* (left) or IT PBS (right) and either an isotype control antibody or anti-Ly6G-depleting antibodies prior to tumor inoculation and throughout the experiment (n=5 mice/group from one of two independent experiments).

For all plots, *P<0.05, **P<0.01, ***P<0.001 by one-way Anova (B, F) or two-way ANOVA (C, E), mean ± s.e.m for *in vivo* experiments (E) or mean ± s.d. for *in vitro* experiments (B-C, G).

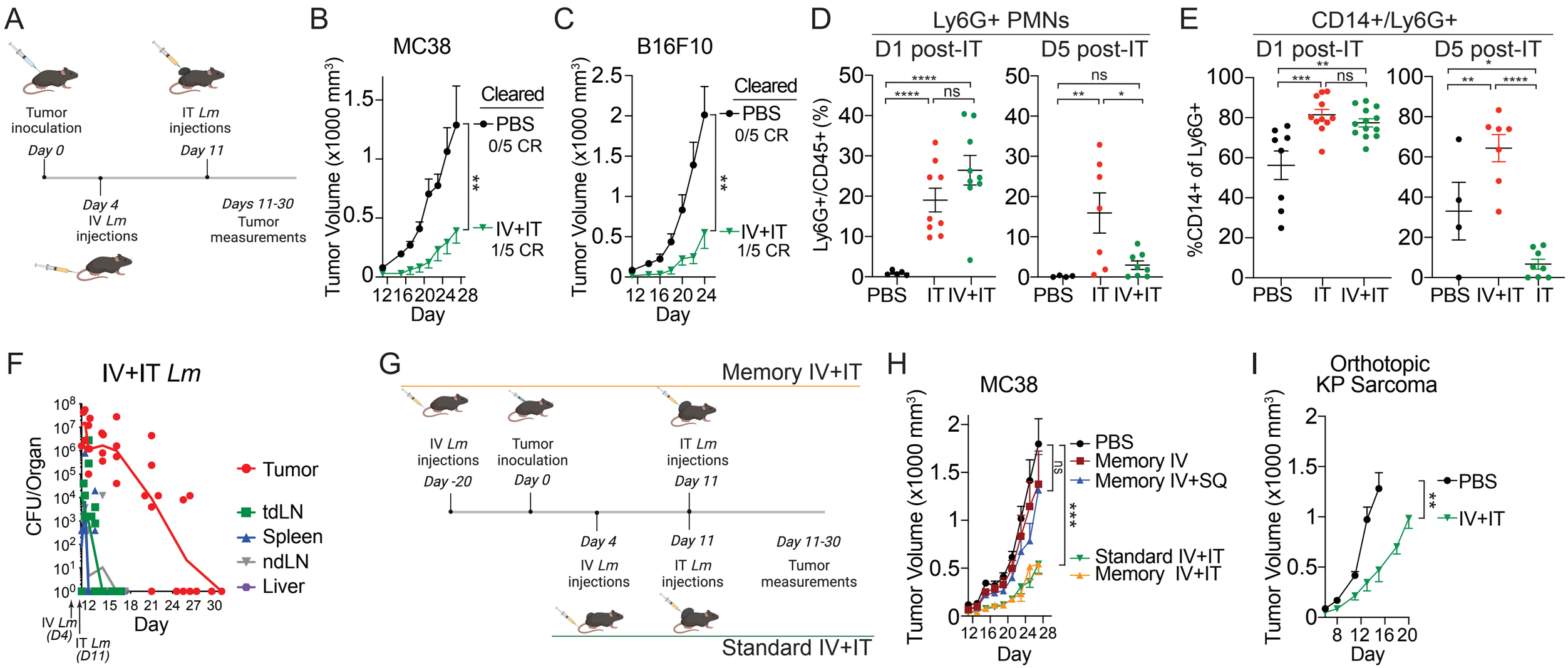

Garcia Castillo, J., Campbell, T., & Fernandez, S. et al. Figure 4.

Figure 4 | IV+IT *Lm* controls multiple tumor types while clearing intratumoral bacteria and PMN-MDSCs from tumors.

(A) Experimental strategy for IV+IT *Lm* dosing regimen.

(B-C) IV+IT PBS versus IV+IT *Lm* regimen and growth of MC38 (B, data shown from n= 4-5 mice per group from one of three experiments) and B16F10 (C, data shown from n= 5-6 mice per group from one of two experiments) tumors.

(D) Frequency of $Ly6G^+$ PMNs of all $CD45^+$ cells one day (left) and 5 days (right) after *Lm* IT in IV+IT *Lm* regimen (data shown from n= 5 mice per group from two pooled experiments).

(E) Percent of $Ly6G^+$ PMNs that were $CD14^+$ 1 day (left) and 5 days (right) after IT *Lm* in IV+IT *Lm* regimen.

(F) CFU analysis for *Lm* after IV+IT *Lm* regimen in MC38 tumor-bearing mice. Organs were harvested 4 hours, 12 hours, and on days 1, 3, 5, 10, 15, and 20 after IT *Lm* administration.

(G) Experimental design for comparing prophylactic IV Lm (memory IV+IT) to standard IV+IT *Lm* dosing regimen.

(H) MC38 tumor growth in the setting of memory IV+IT, memory IV only, and memory IV+SubQ *Lm* (injected on opposing flank) compared to PBS treatment or standard IV+IT *Lm*.

(I) Orthotopic KP sarcoma growth with PBS versus a memory IV+IT *Lm* dosing regimen.

For all plots, *P<0.05, **P<0.01, ***P<0.001 by student t-test (C, D, E) or two-way ANOVA (B, C, H, I), mean ± s.e.m.

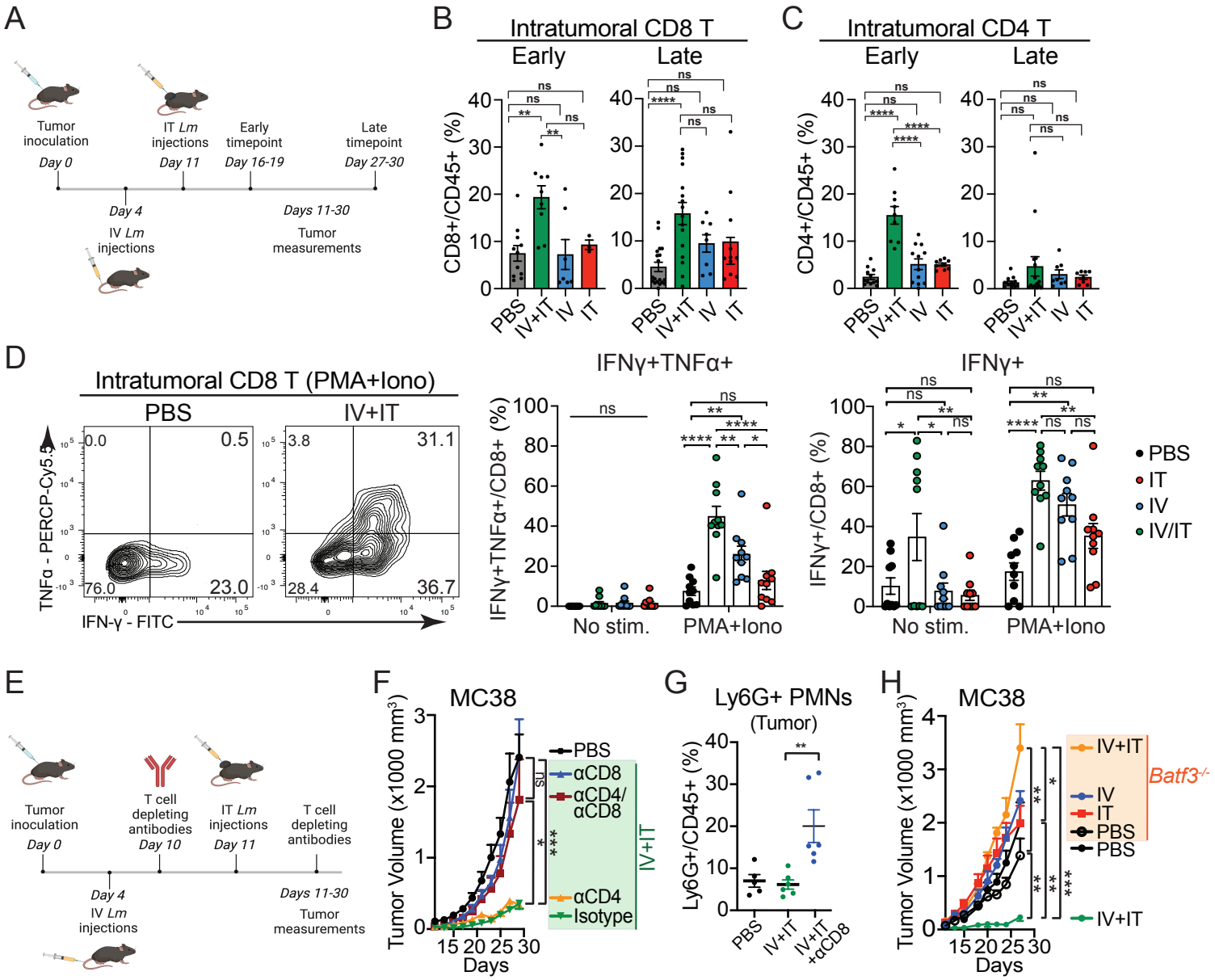

Garcia Castillo, J., Campbell, T., & Fernandez, S. et al. Figure 5.

Figure 5 | $CD8^+$ T cells are required for tumor control with IV+IT *Lm*.
(A) Experimental strategy for IV+IT *Lm* dosing regimen followed by early or late flow cytometry analysis.
(B-C) Frequency of intratumoral $CD8^+$ (B) or $CD4^+$ (C) T cells of $CD45^+$ cells from MC38 tumors at early (left) or late (right) timepoints as specified in (A) (results pooled from four experiments with 5 mice/group).
(D) Representative flow plots for IFNγ and TNFα intracellular cytokine staining from intratumoral CD8 T cells 8 days after IT *Lm* or IT PBS administration in each *Lm* dosing regimen (results pooled from two experiments with 5 mice/group).
(E) Experimental strategy for IV+IT *Lm* dosing regimen plus anti-CD8, anti-CD4, or both depleting antibodies beginning 10 days after MC38 tumor inoculation.
(F) MC38 tumor growth with T cell depletion.
(G) Frequency of intratumoral $Ly6G^+$ PMNs of $CD45^+$ cells in IV+IT *Lm* treated mice +/- anti-CD8 depleting antibodies at end of experiment from (F).
(H) MC38 tumor growth in WT versus *Batf3*$^{-/-}$ mice treated with IV+IT *Lm*.
For all plots, *P<0.05, **P<0.01, ***P<0.001 by student t-test (B-C, G), one-way ANOVA (D), or two-way ANOVA (F, H), mean ± s.e.m.

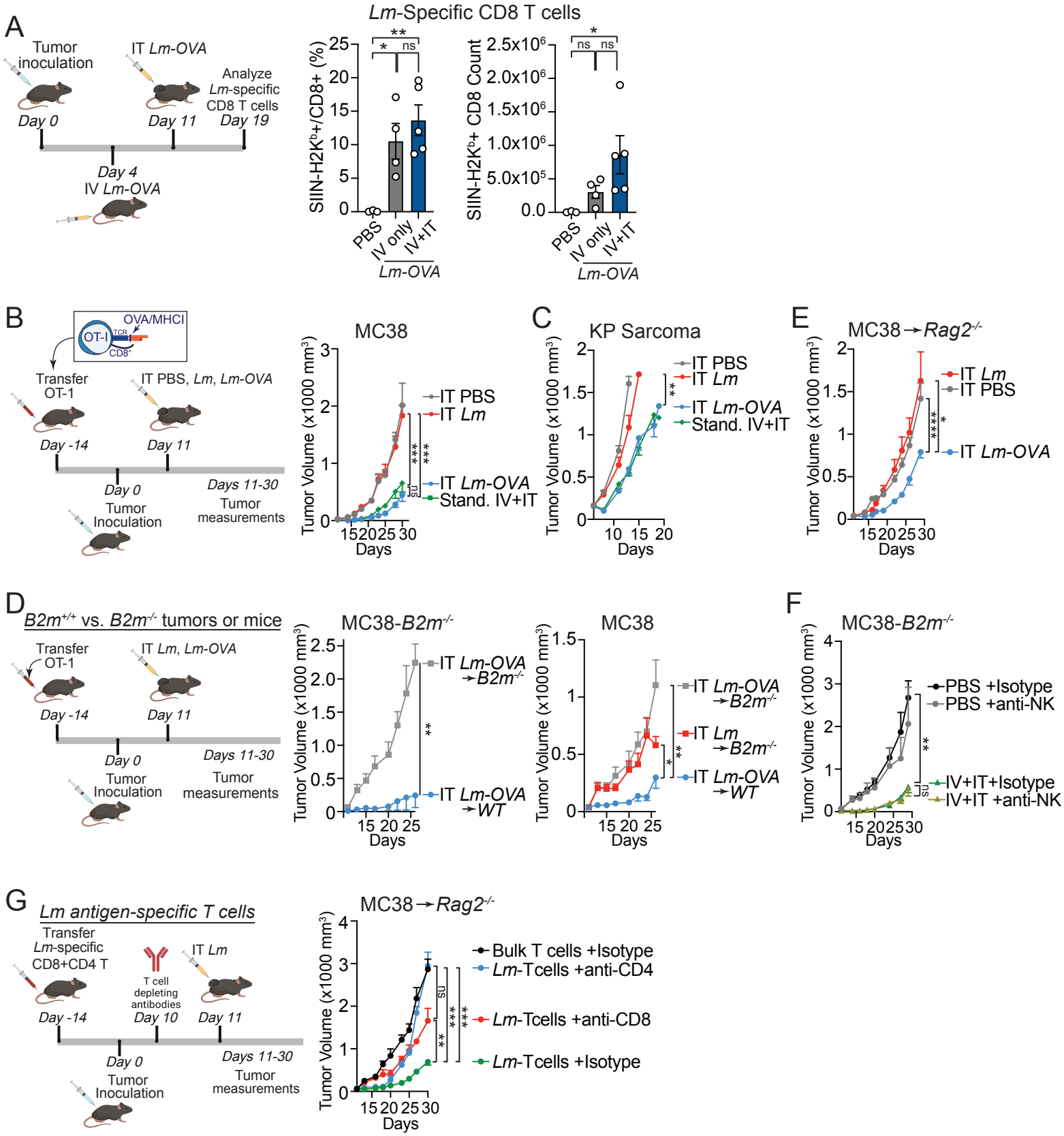

Garcia Castillo, J., Campbell, T., & Fernandez, S.et al. Figure 6.

Figure 6 | Anti-*Listeria* CD8 immunity mediates tumor control.
(A) Experimental design to analyze *Lm*-specific CD8 T cells after IV+IT *Lm* (right) frequency (middle) and total number (left) of *Lm*-specific (SIIN-H2K^b tetramer) CD8 T cells from MC38 tumors 8 days after IT *Lm-OVA* in IV+IT *Lm-OVA* regimen. OVA was expressed from *Lm* as a surrogate *Lm* antigen.
(B) Experimental strategy to adoptively transfer *in vitro*-activated OT-I CD8 T cells in place of prophylactic IV *Lm* and MC38 tumors measured after IT PBS, *Lm*, or *Lm-OVA* (n= 5-6 mice/group from one of two experiments).
(C) As in (B) but using an orthotopic KP sarcoma model (n= 5-6 mice/group from one of two independent experiments).
(D) As in (B) but IT delivery compared MC38 tumors grown in WT or β2m$^{-/-}$ mice (left) or MC38-*B2m*$^{-/-}$ tumors grown in WT or β2m$^{-/-}$ mice (right) (n= 5-6 mice per group).
(E) As in (B) but in *Rag2*$^{-/-}$ mice (n= 5-6 mice/group).
(F) MC38-B2m$^{-/-}$ tumor growth after IV+IT *Lm* or IV+IT PBS plus anti-NK1.1 beginning 10 days after MC38-B2m$^{-/-}$ tumor inoculation (n= 5-6 mice/group).
(G) Experimental strategy to adoptively transfer *in vitro*-activated *Lm*-specific CD8 and CD4 T cells in place of prophylactic IV *Lm* and MC38 tumors measured after IT PBS or *Lm* plus anti-CD8 or anti-CD4 beginning 10 days after MC38 tumor inoculation (n= 5-6 mice/group from one of two experiments).
For all plots, *P<0.05, **P<0.01, ***P<0.001 by student t-test (A) or two-way ANOVA (B-G), mean ± s.e.m.

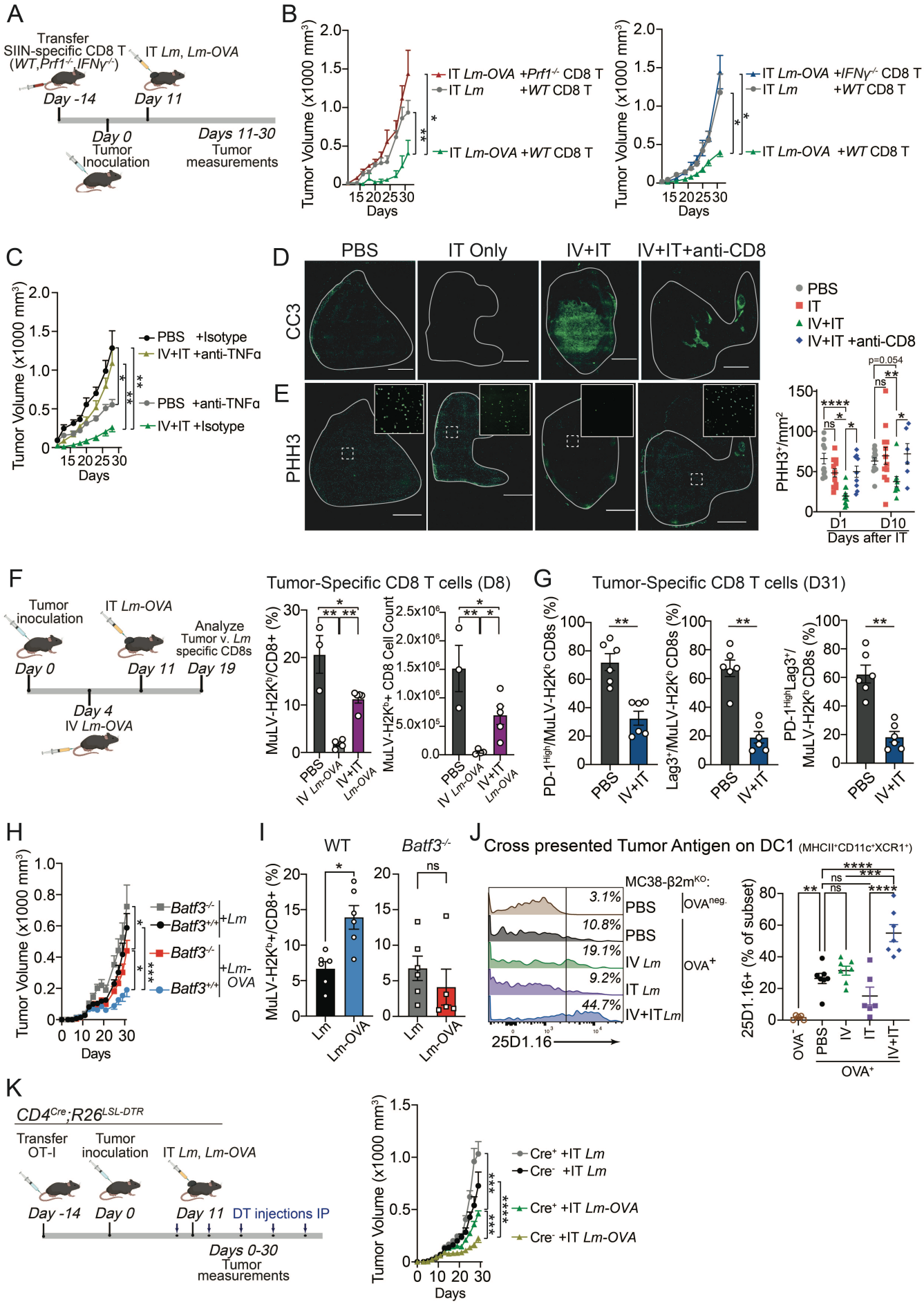

Garcia Castillo, J., Campbell, T., & Fernandez, S.et al. Figure 7.

Figure 7 | Anti-*Listeria* CD8 immunity enhances antitumor responses.
(A) Experimental strategy to adoptively transfer *in vitro* expanded SIIN-specific CD8 T cells from WT, *Prf1*$^{-/-}$, *IFNγ*$^{-/-}$ mice immunized with *Lm-OVA* (see methods).
(B) MC38 tumor growth after adoptive transfer of SIIN-specific CD8 T cells from WT, IFNγ$^{-/-}$, or *Prf1*$^{-/-}$ mice followed by IT injection of PBS, *Lm*, or *Lm-OVA* at day 11 of tumor growth (n= 6 mice/group from one of two experiments).
(C) MC38 tumor growth plus anti-TNFα beginning 10 days after MC38-B2m$^{-/-}$ tumor inoculation (n= 5-6 mice/group from one of two experiments)
(D) Representative images of Cleaved-Caspase 3 (CC3) (green) in MC38 tumors 24 hours post injection with IT PBS, IT *Lm*, or IV+IT *Lm* +/- anti-CD8 i.p. Scale bar = 2000μm. See Fig S7 for additional stains and day 10 images.
(E) Representative images of phospho-Histone 3 (PHH3) (green) in MC38 tumors 24 hours post injection with IT PBS, IT *Lm*, IV+IT *Lm* +/- anti-CD8 i.p. and quantification of PHH3 staining in MC38 tumors in each group 1 day and 10 days after IT injections. Scale bar = 2000μm. Inset = high resolution images of boxed section of tissue. See Fig S7 for additional stains and day 10 images.
(F) Experimental design for the analysis of frequency (left) and total number (right) of tumor-specific CD8 T cells (MuLV-H2K^{b} tetramer) 8 days after IT *Lm-OVA* in IV+IT *Lm-OVA* regimen compared to IV+IT PBS or IV *Lm-OVA* only.
(G) Frequency of PD-1^{High} (left), Lag3^{+}(center), and PD-1^{High}Lag3^{+} double-positive (right) tumor-specific (MuLV-H2K^{b} tetramer) CD8 T cells from MC38 tumors 31 days after PBS or IV+IT *Lm*.
(H) In vitro activated OT-I CD8 T cells were adoptively transferred into WT or *Batf3*$^{-/-}$ mice, MC38 tumors inoculated, and then tumors were injected IT on day 11 with *Lm* or *Lm*-OVA and tumor growth monitored (n= 5-6 mice per group pooled from two experiments).
(I) Frequency of tumor-specific (MuLV-H2K^{b} tetramer) CD8 T cells from tumors at end of experiment in (H).
(J) Representative histogram plots and quantification of 25D1.16 staining (anti-SIIN-H2K^{b}) on intratumoral cDC1s (MHCII^{+}CD11c^{+}XCR1^{+}) in OVA-expressing *B2m*-deficient MC38 tumors 24 hours post IT PBS, IT *Lm*, or IV+IT *Lm*.
(K) Adoptive transfer of *Lm*-specific OT-I T cells (as in Figure 6B) was done into T cell depleter mice (*CD4-Cre; R26*$^{LSL-DTR}$) that were treated with DT beginning 10 days after MC38 tumor inoculation and tumor growth was monitored (n= 5-6 mice per group pooled from two experiments).
For all plots, *P<0.05, **P<0.01, ***P<0.001 by student t-test (F-G, I) or two-way ANOVA (B-C, H, J), mean ± s.e.m.